Article

Neuron

A Visual Circuit Related to Habenula Underlies the Antidepressive Effects of Light Therapy

Graphical Abstract

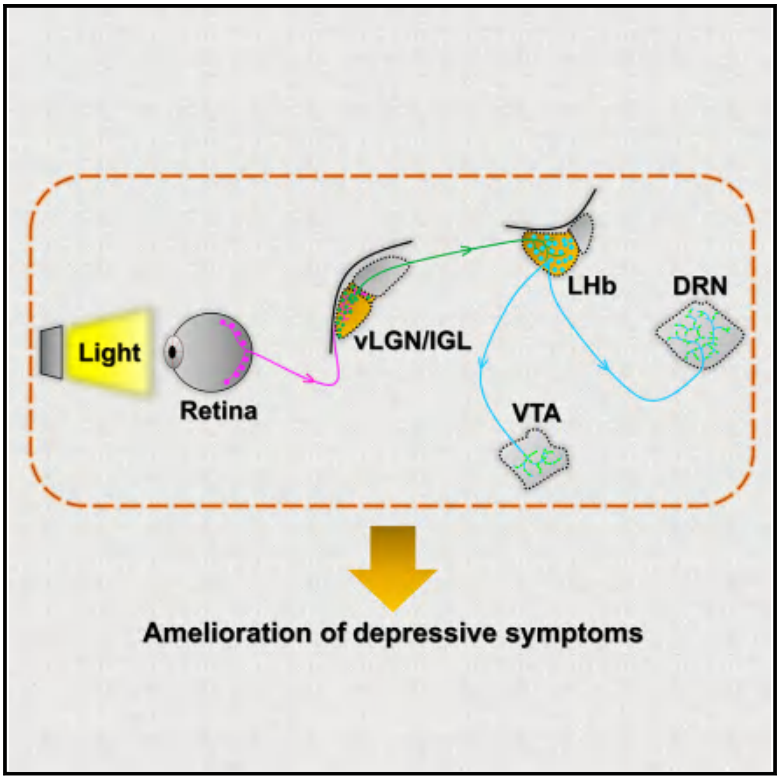

Authors

Lu Huang, Yue Xi, Yanfang Peng, ..., Minmin Luo, Kwok-Fai So, Chaoran Ren

Correspondence

tchaoran@jnu.edu.cn

In Brief

Huang et al. identified a visual circuit related to the LHb that regulates depressive-like behaviors. They demonstrate that activation of the disynaptic retina-vLGN/IGL-LHb pathway underlies the antidepressive effects of light therapy.

Highlights

- Activation of LHb-projecting vLGN/IGL neurons inhibits neuronal activity in the LHb
- M4-type mRGCs directly innervate the vLGN/IGL-LHb pathway
- Activation of the retina-vLGN/IGL-LHb pathway decreases depressive-like behaviors
- Light therapy ameliorates depressive symptoms via the retina-vLGN/IGL-LHb pathway

Huang et al., 2019, Neuron 102, 1–15
April 3, 2019
https://doi.org/10.1016/j.neuron.2019.01.037

CellPress

Please cite this article in press as: Huang et al., A Visual Circuit Related to Habenula Underlies the Antidepressive Effects of Light Therapy, Neuron (2019), https://doi.org/10.1016/j.neuron.2019.01.037

Neuron
Article

A Visual Circuit Related to Habenula Underlies the Antidepressive Effects of Light Therapy

Lu Huang,[1,2,13] Yue Xi,[1,13] Yanfang Peng,[1] Yan Yang,[1] Xiaodan Huang,[1,13] Yunwei Fu,[1] Qian Tao,[3] Jia Xiao,[4] Tifei Yuan,[5] Kai An,[6] Huan Zhao,[6] Mingliang Pu,[7] Fuqiang Xu,[8] Tian Xue,[6] Minmin Luo,[9] Kwok-Fai So,[1,10,11,12,13] and Chaoran Ren[1,10,12,14,*]

[1]Guangdong-Hongkong-Macau Institute of CNS Regeneration, Ministry of Education CNS Regeneration Collaborative Joint Laboratory, Jinan University, Guangzhou 510632, China
[2]Department of Neurology and Stroke Center, The First Affiliated Hospital of Jinan University, Guangzhou 510632, China
[3]Psychology Department, School of Medicine, Jinan University, Guangzhou 510632, China
[4]Clinical Medicine Research Institute, The First Affiliated Hospital of Jinan University, Guangzhou 510632, China
[5]Shanghai Mental Health Center, Shanghai Jiaotong University School of Medicine, Shanghai 200030, China
[6]Hefei National Laboratory for Physical Sciences at the Microscale, Neurodegenerative Disorder Research Center, Chinese Academy of Sciences Key Laboratory of Brain Function and Disease, School of Life Sciences, Division of Life Sciences and Medicine, University of Science and Technology of China, Hefei 230026, China
[7]Department of Anatomy, School of Basic Medical Sciences, Peking University, Beijing 100191, China
[8]State Key Laboratory of Magnetic Resonance and Atomic and Molecular Physics, Wuhan Institute of Physics and Mathematics, Center for Excellence in Brain Science and Intelligent Technology, Chinese Academy of Sciences, Wuhan 430071, China
[9]National Institute of Biological Sciences, Zhongguancun Life Science Park 7 Science Park Road, Beijing 102206, China
[10]Guangzhou Regenerative Medicine and Health Guangdong Laboratory, Guangzhou 510530, China
[11]Department of Ophthalmology and State Key Laboratory of Brain and Cognitive Sciences, The University of Hong Kong, Hong Kong, China
[12]Co-innovation Center of Neuroregeneration, Nantong University, Nantong 226001, China
[13]These authors contributed equally
[14]Lead Contact
*Correspondence: tchaoran@jnu.edu.cn
https://doi.org/10.1016/j.neuron.2019.01.037

SUMMARY

Light plays a pivotal role in the regulation of affective behaviors. However, the precise circuits that mediate the impact of light on depressive-like behaviors are not well understood. Here, we show that light influences depressive-like behaviors through a disynaptic circuit linking the retina and the lateral habenula (LHb). Specifically, M4-type melanopsin-expressing retinal ganglion cells (RGCs) innervate GABA neurons in the thalamic ventral lateral geniculate nucleus and intergeniculate leaflet (vLGN/IGL), which in turn inhibit CaMKIIa neurons in the LHb. Specific activation of vLGN/IGL-projecting RGCs, activation of LHb-projecting vLGN/IGL neurons, or inhibition of postsynaptic LHb neurons is sufficient to decrease the depressive-like behaviors evoked by long-term exposure to aversive stimuli or chronic social defeat stress. Furthermore, we demonstrate that the antidepressive effects of light therapy require activation of the retina-vLGN/IGL-LHb pathway. These results reveal a dedicated retina-vLGN/IGL-LHb circuit that regulates depressive-like behaviors and provide a potential mechanistic explanation for light treatment of depression.

INTRODUCTION

Light signals transmitted by the retina are a powerful modulator of mood-related behaviors (LeGates et al., 2014). Clinical evidence supports an antidepressive effect of light therapy (Rosenthal et al., 1984; Kripke, 1998; Golden et al., 2005; Wirz-Justice et al., 2009, 2011; Lieverse et al., 2011; Lam et al., 2016; Sit et al., 2018), while light deprivation can increase depressive-like behaviors across species (Wilson, 2002; Gonzalez and Aston-Jones, 2008; Monje et al., 2011; Lau et al., 2011). Unveiling the structure and function of neural circuits related to the retina is crucial for understanding how light exerts its influence on depressive-like behaviors.

The lateral habenula (LHb), part of the epithalamus, is a highly conserved nucleus across species, and it regulates the flow of information from the limbic system to the midbrain monoaminergic centers (Hikosaka et al., 2008). Aversive stimuli (AS) can activate the LHb and lead to increases in depressive-like behaviors (Matsumoto and Hikosaka, 2007; Li et al., 2013; Proulx et al., 2014; Lecca et al., 2016; Yang et al., 2018), whereas inhibition of the LHb ameliorates depressive symptoms (Proulx et al., 2014). Recent studies conducted in rodents have suggested that light can influence neuronal activity in the LHb, accompanied by changes in depressive-like behaviors (Zhao and Rusak, 2005; LeGates et al., 2014). However, the visual circuits related to the LHb that regulate depressive-like behaviors remain incompletely understood.

Here, by combining conventional neurotracer and transneuronal virus tracing techniques, we identified a disynaptic visual

circuit connecting the retina and LHb in the mouse. In the retina, a subset of M4-type retinal ganglion cells (RGCs) innervate GABA neurons in the ventral lateral geniculate nucleus and intergeniculate leaflet (vLGN/IGL), which in turn inhibit the neural activity of the LHb. The role of the retina-vLGN/IGL-LHb pathway in the regulation of depressive-like behaviors was investigated using an array of brain circuit interrogation tools, including fiber photometry, c-Fos brain mapping, and chemogenetics. We demonstrate that the activation of the retina-vLGN/IGL-LHb pathway is required for the antidepressive effects of bright light therapy.

RESULTS

vLGN/IGL Neurons Inhibit the LHb through Direct Projections

Results derived from the mouse mesoscale connectome suggest that GABA neurons in the vLGN/IGL project to the LHb (Oh et al., 2014). To further determine the distribution pattern and identity of LHb-projecting vLGN/IGL neurons, we first delivered a Cre-dependent virus encoding a red fluorescent protein, mCherry (AAV2/9-DIO-mCherry), into the vLGN/IGL of vGAT-Cre mice to selectively infect GABA neurons, after which we injected the LHb with green fluorescent latex microspheres (retrobeads) to retrogradely label LHb-projecting vLGN/IGL neurons (Figure S1A). We found that LHb-projecting vLGN/IGL neurons labeled with retrobeads were mainly distributed in the external part of the vLGN and IGL, in which ~93.88% of retrobead-labeled LHb-projecting neurons were co-labeled with mCherry (Figure S1A). It is well established that most LHb neurons are excitatory (Aizawa et al., 2012). To determine whether vLGN/IGL neurons specifically target LHb excitatory neurons, we delivered the monosynaptic anterograde transport virus AAV2/1-Cre (Zingg et al., 2017) into the vLGN/IGL and a Cre-dependent virus encoding the yellow fluorescent protein EYFP (AAV2/9-DIO-EYFP) into the LHb of C57BL/6 mice (Figure S1B). Approximately 99.33% of the LHb postsynaptic neurons expressing EYFP were immunoreactive for CaMKIIa (Figure S1B), indicating the excitatory nature of these cells. To identify the projection targets of the LHb postsynaptic neurons, we first labeled axons and presynaptic terminals of LHb postsynaptic neurons by injecting AAV2/1-Cre into the vLGN/IGL and AAV2/9-DIO-tdTomato-T2A-synaptophysin-EGFP into the LHb (Figure S2A). We found that LHb neurons receiving direct vLGN/IGL input could innervate midbrain monoaminergic centers, including the dorsal raphe nuclei (DRN) and ventral tegmental area (VTA) (Figures S2B–S2D). Next, we infected LHb postsynaptic neurons with AAV2/9-DIO-EYFP and retrogradely labeled DRN-projecting LHb neurons and VTA-projecting LHb neurons by injecting red retrobeads into the DRN and VTA, respectively (Figures S2E and S2I). We found that ~39.9% of LHb postsynaptic neurons expressing EYFP projected to the DRN, while 45.6% of LHb postsynaptic neurons expressing EYFP projected to the VTA (Figures S2E–S2L). These results provide direct evidence that a subgroup of vLGN/IGL GABA neurons synapse onto LHb excitatory neurons, which could further project to the DRN and VTA.

To explore the functional contribution of vLGN/IGL-LHb projections, we delivered the monosynaptic retrograde transport virus rAAV2/2-Retro-Cre (Tervo et al., 2016) into the LHb of C57BL/6 mice and a Cre-dependent virus encoding channelrhodopsin-2 and EYFP (AAV2/9-DIO-hChR2(H134R)-EYFP) into the vLGN/IGL (Figures 1A, 1B, and S1C). Next, we optogenetically activated vLGN/IGL-LHb projections and recorded postsynaptic currents from LHb CaMKIIa neurons (Figure 1C). Blue light evoked exclusively inhibitory postsynaptic currents (IPSCs) in 43.8% of recorded neurons, but both IPSCs and excitatory postsynaptic currents (EPSCs) in 39.6% of recorded neurons, in which the amplitude of IPSCs is higher than that of EPSCs (Figures 1C and 1D). Furthermore, we found that the inhibitory effects of vLGN/IGL-LHb projections could be blocked by the $GABA_A$ receptor antagonist SR95531, while the excitatory effects could be blocked by the AMPA/kainate receptor antagonist CNQX (Figure 1E). Finally, we tested the effects of stimulation of vLGN/IGL-LHb projections on the neuronal activity of LHb neurons. Optogenetic activation of ChR2-positive axon terminals inhibited both spontaneous firing and current-evoked action potentials in LHb neurons, and these effects were blocked by the application of SR95531 (Figures 1F and 1G). These results indicate that vLGN/IGL neurons transmit predominantly inhibitory input to LHb CaMKIIa neurons.

Activity of LHb-Projecting vLGN/IGL Neurons Impairs AS-Induced Activation of the LHb

Recent evidence suggests that LHb excitatory neurons encode AS (Li et al., 2013; Lecca et al., 2016; Lawson et al., 2017; Boulos et al., 2017). We postulated that after animals were exposed to AS, the subsequent activation of LHb-projecting vLGN/IGL neurons could attenuate the activation of LHb excitatory neurons. To test this hypothesis, we first injected rAAV2/2-Retro-Cre into the LHb and infected LHb-projecting vLGN/IGL neurons with a Cre-dependent virus encoding the neuronal activator DREADD hM3D (AAV2/9-DIO-hM3D-mCherry) (Figures 2A and 2B). Next, we used fiber photometry (Gunaydin et al., 2014; Wang et al., 2017a) to quantitatively measure AS (foot shock, air puff, fox urine, or physical restraint)-induced changes in Ca^{2+} signals in LHb CaMKIIa neurons expressing the Ca^{2+} indicator GCaMP6m (Figures 2C and 2D). We observed that AS reliably evoked robust activation of LHb CaMKIIa neurons, whereas chemogenetic activation of LHb-projecting vLGN/IGL neurons significantly decreased the excitatory effects of AS (Figures 2E and S3). Together, we demonstrate that neuronal activity of LHb-projecting vLGN/IGL neurons attenuates the activation of LHb excitatory neurons induced by AS.

Activation of the vLGN/IGL-LHb Pathway Decreases Depressive-like Behaviors

Recent studies imply that increased aberrant LHb neuronal activity (e.g., hyperexcitability and increases in burst firing) induced by long-term exposure to AS leads to an increase in depressive-like behaviors (Li et al., 2013; Lecca et al., 2016; Lawson et al., 2017; Boulos et al., 2017; Yang et al., 2018). This prompted us to explore the influence of LHb-projecting vLGN/IGL neurons on the depressive-like behaviors and aberrant activity of LHb neurons induced by long-term exposure to AS. We delivered rAAV2/2-Retro-Cre into the bilateral LHb and infected LHb-projecting vLGN/IGL neurons with AAV2/9-DIO-hM3D-mCherry or

Please cite this article in press as: Huang et al., A Visual Circuit Related to Habenula Underlies the Antidepressive Effects of Light Therapy, Neuron (2019), https://doi.org/10.1016/j.neuron.2019.01.037

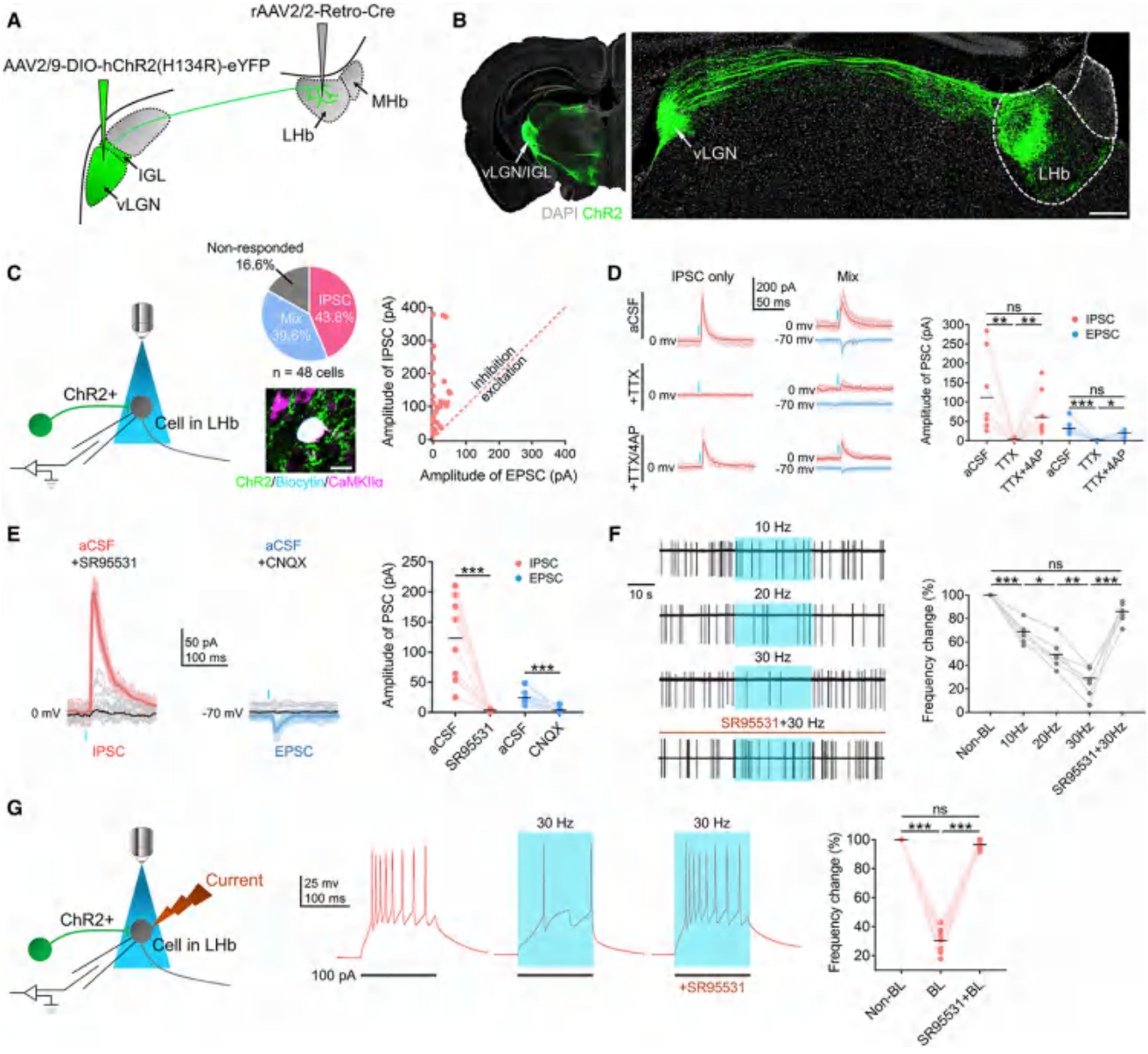

Figure 1. vLGN/IGL Neurons Inhibit the LHb through Direct Projections

(A) Scheme for specific labeling of LHb-projecting vLGN/IGL neurons with ChR2.

(B) Representative images of the vLGN/IGL and LHb 2 weeks after virus injections.

(C) Left: scheme for recording the postsynaptic currents in LHb CaMKIIa neurons evoked by optogenetic activation of vLGN/IGL-LHb projections. Middle top: light-evoked synaptic responses in LHb neurons. Pie chart indicates whether the absolute amplitude was greater for evoked IPSC, IPSC and EPSC (Mix), or no response. Middle bottom: a recorded LHb CaMKIIa neuron filled with biocytin. Right: absolute amplitude of blue-light-evoked IPSCs and EPSCs of LHb neurons (n = 37 cells).

(D) Light-evoked postsynaptic currents were completely blocked by application of tetrodotoxin (TTX) and recovered by application of TTX/4AP, indicating that the postsynaptic currents recorded in LHb neurons were elicited by direct synaptic connections between LHb-projecting vLGN/IGL neurons and the recorded LHb neurons.

(E) Light-evoked IPSCs were blocked by application of SR95531, while EPSCs were blocked by application of CNQX.

(F and G) Optogenetic activation of vLGN/IGL-LHb projections reduced spontaneous firing (F) and the number of action potentials related to current injection (G) in LHb neurons, and those effects were blocked by application of SR95531.

Scale bars represent 200 mm (B) and 10 mm (C). For all figures, *p < 0.05, **p < 0.001, ***p < 0.0001, and ns, no significant difference (one-way ANOVA with Sidak's multiple comparisons test). Dot plots include horizontal lines indicating the mean. See also Figures S1 and S2.

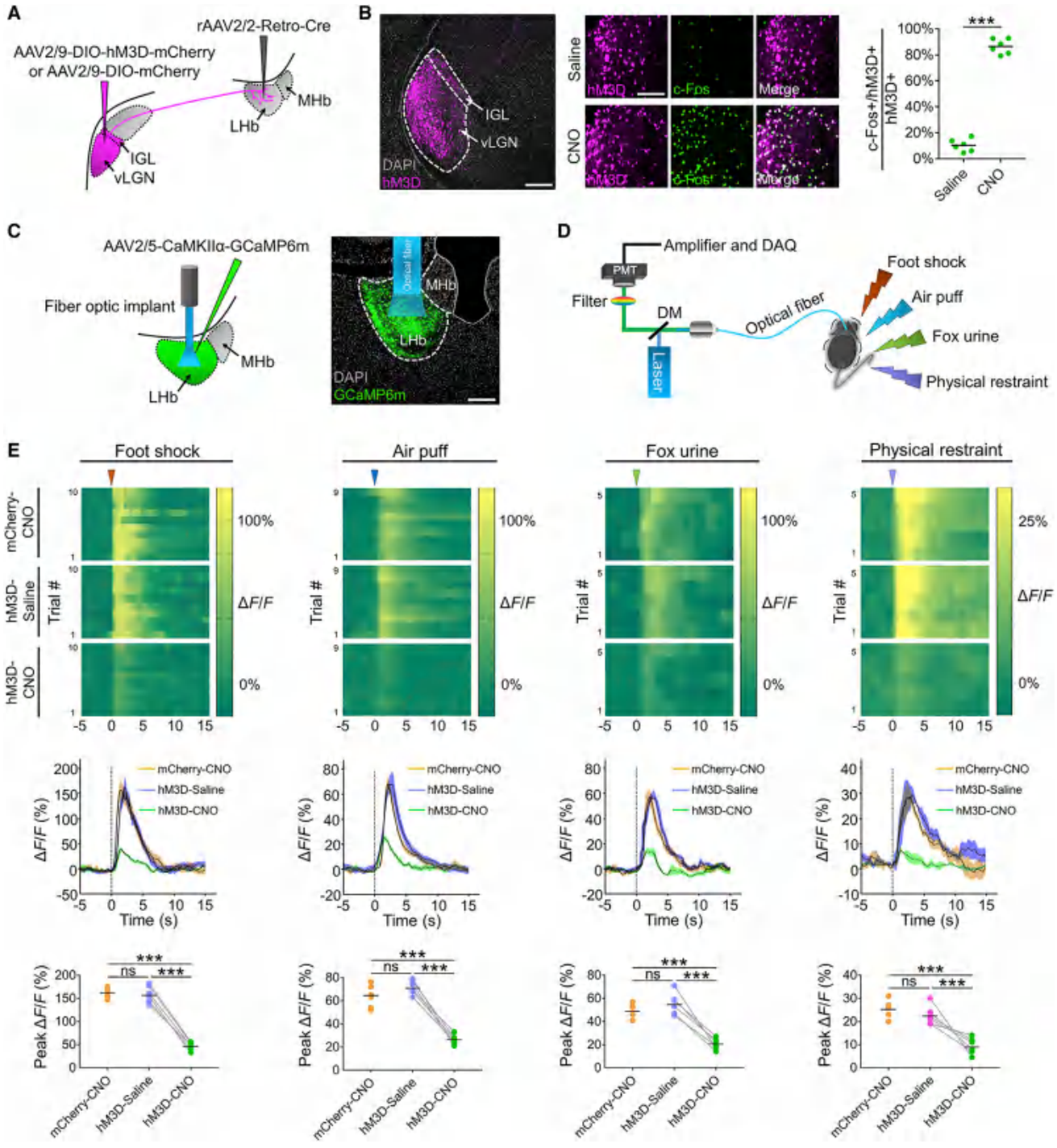

Figure 2. Specific Activation of LHb-Projecting vLGN/IGL Neurons Impairs Excitatory Effects of AS onto LHb CaMKIIa Neurons

(A) Scheme for specific infection of LHb-projecting vLGN/IGL neurons with hM3D or mCherry.

(B) Left: representative images of the vLGN/IGL showing that i.p. injection of saline or CNO evoked c-Fos expression in neurons expressing hM3D. Right: percentage of total hM3D cells expressing c-Fos in different groups (n = 6 animals/group).

(C) Left: AAV2/5-CaMKIIa-GCaMP6m was injected into the LHb; subsequently, a 230-mm fiber optic implant was implanted in the LHb. Right: representative image of the LHb 2 weeks after AAV2/5-CaMKIIa-GCaMP6m injection.

(D) Scheme of the fiber photometry apparatus used to measure AS-evoked Ca^{2+} signals in LHb CaMKIIa neurons.

(E) Top (mCherry-CNO): heatmaps showing the Ca^{2+} signals evoked by foot shock (10 trials), air puff (9 trials), fox urine (5 trials), and physical restraint (5 trials) in LHb CaMKIIa neurons from a CNO-treated C57BL/6 mouse whose LHb-projecting vLGN/IGL neurons were infected with mCherry. Top (hM3D-Saline): heatmaps

(legend continued on next page)

AAV2/9-DIO-mCherry (Figures 3A and 3B). After 28 days of exposure to AS (foot shock, 20 times/day; air puff, 20 times/day; fox urine, 30 min/day; physical restraint, 1 h/day), mice were subjected to a battery of depression- and anxiety-related behavioral tests (Figure 3A). Long-term exposure to AS significantly increased depressive-like behaviors tested in the sucrose preference test (SPT), forced swimming test (FST), and shuttle box test (SBT) (Figure 3C) and anxiety-like behaviors tested in the open field test (OFT), elevated plus maze test (EPM), and novelty-suppressed feeding test (NSF) (Figure S4A). By contrast, the locomotor activities of these mice were not significantly different (Figure S4A), which indicated that the increased depressive- and anxiety-like behaviors were not due to motor defects. Moreover, depressive-like behaviors were reversed by antidepressant treatment (fluoxetine, injected intraperitoneally [i.p.] at 10 mg/kg daily for 14 days) (Figure 3C). Furthermore, we found that LHb neurons from mice with long-term exposure to AS exhibited a higher number of action potentials in response to current injections, an elevated spontaneous firing rate, and increased burst firing (Figures 3D, 3E, and S4B), indicating that long-term exposure to AS increased the excitability and burst firing of LHb neurons.

We next investigated the influence of the activation of LHb-projecting vLGN/IGL neurons on depressive-/anxiety-like behaviors and the aberrant activity of LHb neurons. During the last 14 days of exposure to AS, LHb-projecting vLGN/IGL neurons infected with hM3D-mCherry were activated daily via i.p. injection of clozapine N-oxide (CNO) (2 mg/kg) (Figure 3A). Activation of LHb-projecting vLGN/IGL neurons significantly decreased depressive- and anxiety-like behaviors, and this decrease was accompanied by significantly reduced excitability and burst firing in the LHb (Figures 3C–3E, S4A, and S4B).

In addition to the LHb, vLGN/IGL GABA neurons can also project to other mood-related nuclei, including the suprachiasmatic nucleus and superior colliculus (Oh et al., 2014). The antidepressive and anxiolytic effects of chemogenetic activation of LHb-projecting vLGN/IGL neurons might be due to altered functions in related brain regions other than the LHb. To determine whether the specific activation of the vLGN/IGL-LHb pathway is sufficient to decrease depressive- and anxiety-like behaviors, we next injected AAV2/1-Cre into the bilateral vLGN/IGL and infected LHb postsynaptic neurons with a Cre-dependent virus encoding the neuronal inhibitor DREADD hM4D (AAV2/9-DIO-hM4D-mCherry) (Figure 3F). During the last 14 days of exposure to AS, LHb neurons expressing hM4D-mCherry were inhibited daily via i.p. injection of CNO (Figures 3A and S4C). We found that specific inhibition of LHb postsynaptic neurons also significantly decreased depressive- and anxiety-like behaviors, accompanied by reduced excitability and burst firing of LHb neurons (Figures 3G–3I, S4D, and S4E). Thus, activation of the vLGN/IGL-LHb pathway is sufficient to ameliorate depressive and anxiety-like symptoms induced by long-term exposure to AS.

Given that activation of the vLGN/IGL-LHb pathway during the last 14 days of exposure to AS corresponds to a prevention protocol rather than a treatment protocol for depression, we next tested whether activation of the vLGN/IGL-LHb pathway could reverse depressive symptoms after the induction of depression by AS. We used a 38-day protocol in which 10 days of daily chemogenetic activation of the LHb-projecting vLGN/IGL neurons expressing hM3D-mCherry or inhibition of the LHb postsynaptic neurons expressing hM4D-mCherry was conducted after exposing the mice to 28 days of AS (Figure S5A). We found that both the activation of LHb-projecting vLGN/IGL neurons and the inhibition of LHb postsynaptic neurons reversed the depressive and anxiety-like symptoms induced by long-term exposure to AS (Figures S5B and S5C).

It is widely accepted that exposure to chronic social defeat stress (CSDS) could increase depressive-like behaviors in mice (Berton et al., 2006; Golden et al., 2011), and a recent study found that social attack intensively activated the LHb (Wang et al., 2017a). Next, we further examined the antidepressive and anxiolytic effects of the vLGN/IGL-LHb pathway in a CSDS mouse model. To determine whether the activation of the vLGN/IGL-LHb pathway could prevent the behavioral deficits induced by exposure to CSDS, we exposed the mice to 10 days of SDS and daily activated LHb-projecting vLGN/IGL neurons expressing hM3D-mCherry or inhibited LHb postsynaptic neurons expressing hM4D-mCherry via i.p. injection of CNO (Figure S6A). Both the activation of LHb-projecting vLGN/IGL neurons and the inhibition of LHb postsynaptic neurons significantly decreased depressive-like behaviors tested in the social interaction test (SI) and SPT, as well as anxiety-like behaviors tested in the EPM and NSF, and these changes were accompanied by reduced excitability and burst firing in the LHb (Figures S6B–S6G). To determine whether the activation of the vLGN/IGL-LHb pathway could reverse the behavioral deficits induced by exposure to CSDS, we used a 20-day protocol in which 10 days of daily chemogenetic activation of LHb-projecting vLGN/IGL neurons or inhibition of LHb postsynaptic neurons was conducted after exposing the mice to 10 days of SDS (Figure S7A). We found that both the activation of LHb-projecting vLGN/IGL neurons and the inhibition of LHb postsynaptic neurons reversed depressive- and anxiety-like behaviors (Figures S7B and S7C). Together, these observations indicate that activation of the vLGN/IGL-LHb pathway is also able to alleviate the depressive- and anxiety-like symptoms induced by exposure to CSDS.

M4-type mRGCs Directly Innervate the vLGN/IGL-LHb Pathway

It is well established that RGCs project to the vLGN/IGL (Harrington, 1997). To determine whether LHb-projecting vLGN/IGL

showing the Ca^{2+} signals in LHb CaMKIIa neurons from a saline-treated C57BL/6 mouse whose LHb-projecting vLGN/IGL neurons were infected with hM3D-mCherry. Top (hM3D-CNO): heatmaps showing the Ca^{2+} signals in LHb CaMKIIa neurons from the same mouse used in the hM3D-saline group, which received i.p. injection of CNO. Middle: averaged responses of mice in different groups. Bottom: activation of LHb-projecting vLGN/IGL neurons significantly reduced the amplitude of Ca^{2+} signals associated with exposure to AS (n = 6 animals/group).

Scale bars represent 200 mm (B, left, and C), 100 mm (B, middle). For all figures, ***p < 0.0001 and ns, no significant difference (one-way ANOVA with Sidak's multiple comparisons test). Dot plots include horizontal lines indicating the mean. See also Figure S3.

Please cite this article in press as: Huang et al., A Visual Circuit Related to Habenula Underlies the Antidepressive Effects of Light Therapy, Neuron (2019), https://doi.org/10.1016/j.neuron.2019.01.037

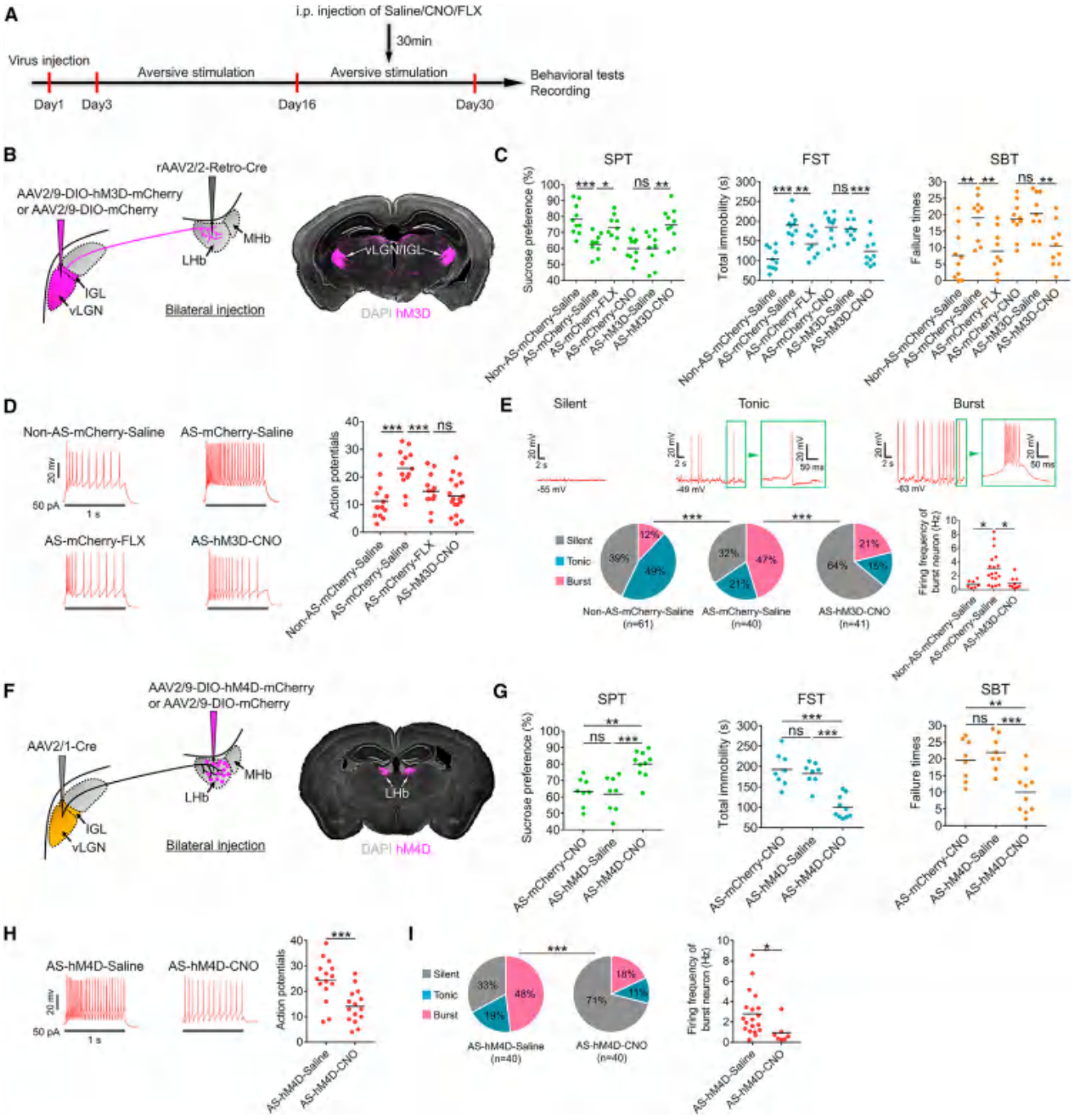

Figure 3. Activation of the vLGN/IGL-LHb Pathway Decreases Depressive-like Behaviors Induced by Long-Term Exposure to AS

(A) Schematic of the experimental design.

(B) Scheme for specific infection of LHb-projecting vLGN/IGL neurons with hM3D or mCherry.

(C) Depressive-like behaviors in different experimental groups (n = 9–10 animals/group). All mice received LHb injection of rAAV2/2-Retro-Cre. Non-AS-mCherry-Saline, mice that received vLGN/IGL injection of AAV2/9-DIO-mCherry, i.p. injection of saline, and no exposure to AS; AS-mCherry-Saline, mice that received vLGN/IGL injection of AAV2/9-DIO-mCherry, i.p. injection of saline, and exposure to AS; AS-mCherry-FLX, mice that received vLGN/IGL injection of AAV2/9-DIO-mCherry, i.p. injection of fluoxetine (FLX), and exposure to AS; AS-mCherry-CNO, mice that received vLGN/IGL injection of AAV2/9-DIO-mCherry, i.p. injection of CNO, and exposure to AS; AS-hM3D-Saline, mice that received vLGN/IGL injection of AAV2/9-DIO-hM3D-mCherry, i.p. injection of saline, and exposure to AS; AS-hM3D-CNO, mice that received vLGN/IGL injection of AAV2/9-DIO-hM3D-mCherry, i.p. injection of CNO, and exposure to AS.

(D) The current-evoked action potentials in brain slices of Non-AS-mCherry-Saline, AS-mCherry-Saline, AS-mCherry-FLX, and AS-hM3D-CNO mice (n = 13–18 cells/group).

(legend continued on next page)

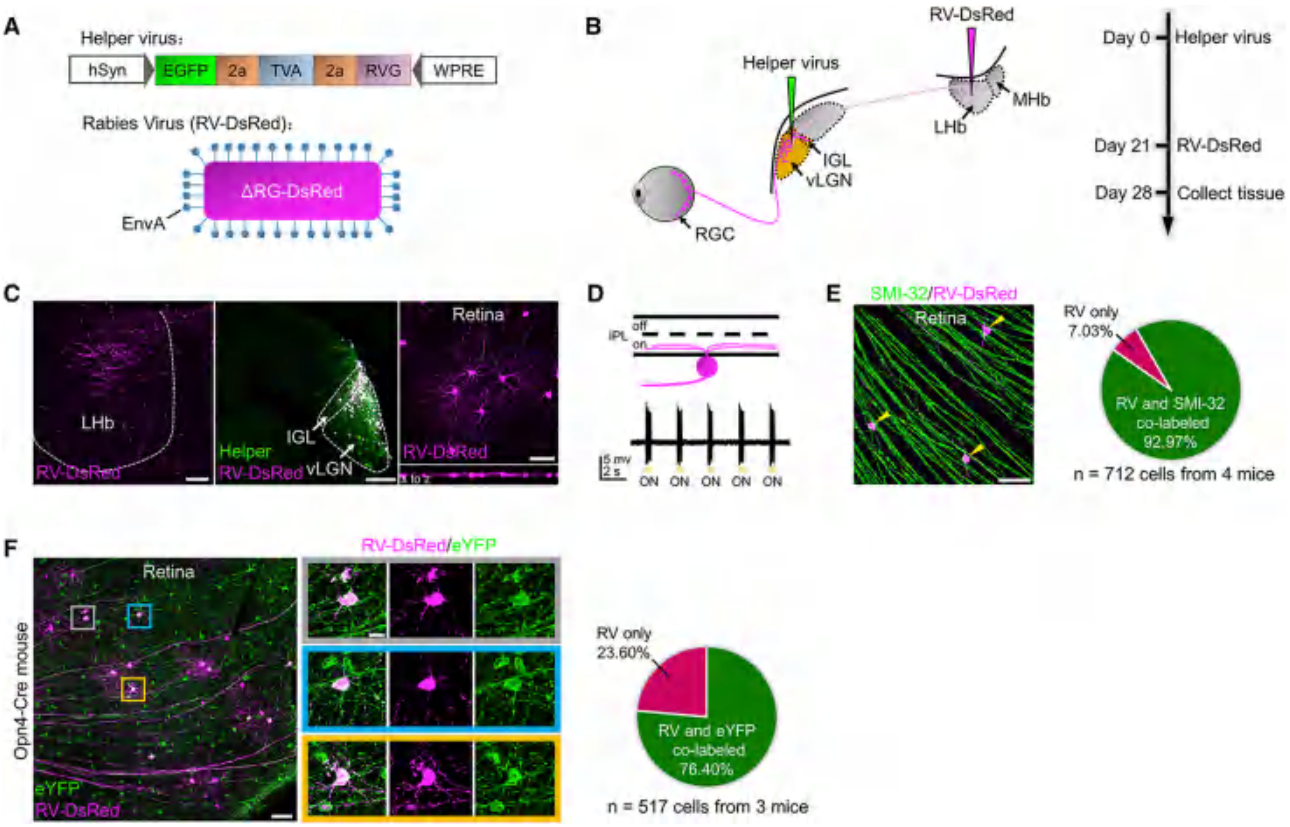

Figure 4. M4-type mRGCs Directly Innervate the vLGN/IGL-LHb Pathway

(A) Design of Helper virus and SAD-DG-DsRed (EnvA).

(B) Experimental design of virus tracing in C57BL/6 mice and Opn4-Cre mice.

(C) Left: LHb injection site. Middle: a representative image of the vLGN/IGL showing the location of starter cells (white). Right: retina of a C57BL/6 mouse showing RV-DsRed-labeled RGCs.

(D) Top: schematic summary of the ramification pattern of RV-DsRed-labeled RGCs. IPL, inner plexiform layer; off, OFF sublamina of the inner plexiform layer; on, ON sublamina of the inner plexiform layer. Bottom: visual response of an RV-DsRed-labeled RGC.

(E) Left: representative image of whole-mount retina of a C57BL/6 mouse showing RV-DsRed-labeled RGCs that were immunopositive for SMI-32. Right: pie chart indicates percentage of RV-DsRed-labeled RGCs co-labeled with SMI-32.

(F) Left: a representative image of whole-mount retina of an Opn4-Cre mouse showing RV-DsRed-labeled RGCs that were co-labeled with mRGCs infected with AAV2/9-DIO-EYFP. Right: pie chart indicates percentage of RV-DsRed-labeled RGCs co-labeled with EYFP.

Scale bars represent 50 mm (C, left and right), 100 mm (C, middle, and E and F, left), 20 mm (F, right). See also Figure S8.

neurons receive direct innervation from RGCs, we used a trans-synaptic tracing method based on a modified rabies virus (Cruz-Martín et al., 2014; Tovote et al., 2016). vLGN/IGL neurons were infected with AAV expressing the rabies glycoprotein and histone-tagged GFP (Helper) (Figures 4A and 4B), which is required for the replication of rabies virus (Pulmanausahakul et al., 2008). Next, we injected SAD-DG-DsRed (EnvA) into the LHb to infect Helper+ LHb-projecting vLGN/IGL neurons via their presynaptic

(E) Top: representative traces showing spontaneous activity of silent, tonic-firing, and burst-firing LHb neurons recorded with whole-cell current clamp. Bottom left: pie charts indicate percentage of the three types of LHb neurons in Non-AS-mCherry-Saline, AS-mCherry-Saline, and AS-hM3D-CNO mice (n = 40–61 cells/group). Bottom right: spontaneous firing frequency of burst neuron recorded with whole-cell current clamp (n = 7–18 cells/group).

(F) Scheme for specific infection of LHb postsynaptic neurons with hM4D or mCherry.

(G) Depressive-like behaviors in different experimental groups (n = 8–10 animals/group). All mice received vLGN/IGL injection of AAV2/1-Cre and exposure to AS. AS-mCherry-CNO, mice that received LHb injection of AAV2/9-DIO-mCherry and i.p. injection of CNO; AS-hM4D-Saline, mice that received LHb injection of AAV2/9-DIO-hM4D-mCherry and i.p. injection of saline; AS-hM4D-CNO, mice that received LHb injection of AAV2/9-DIO-hM4D-mCherry and i.p. injection of CNO.

(H) The current-evoked action potentials in brain slices of AS-hM4D-Saline and AS-hM4D-CNO mice (n = 15 cells/group).

(I) Left: pie charts indicate percentage of the three types of LHb neurons in AS-hM4D-Saline and AS-hM4D-CNO mice (n = 40 cells/group). Right: spontaneous firing frequency of burst neuron recorded with whole-cell current clamp (n = 7–19 cells/group).

For all figures, *p < 0.05, **p < 0.001, ***p < 0.0001, and ns, no significant difference (one-way ANOVA with Sidak's multiple comparisons test [C–E, bottom right, and G–I, right], chi-square test [E, bottom left, and I, left]). Dot plots include horizontal lines indicating the mean. See also Figures S4–S7.

terminals (Figures 4A and 4B). The double-infected rabies-DsRed+/glyco-EGFP+ vLGN/IGL relay neurons (starter cells) produced infectious DG-rabies-DsRed that propagated trans-neuronally to infect the RGCs that form synapses with them (Figure 4B). We observed that starter cells were mainly distributed in the external part of the vLGN and IGL (Figures 4C and S8A). In the retina, ~146 ± 31 RGCs were labeled with rabies virus (n = 6 retinas; Figures 4C, S8A, and S8B). Most of the rabies-virus-labeled RGCs were immunopositive for SMI-32 (92.97%) and exhibited morphological features similar to M4-type melanopsin-expressing RGCs (mRGCs) (Estevez et al., 2012), including large perikarya (20 ± 2 mm, n = 106 cells), trunk-like axons, and radially oriented dendritic processes that stratify in the ON sublamina of the inner plexiform layer (IPL) (Figures 4C–4E). Visual response properties of rabies-virus-labeled RGCs were tested in 21 cells. All cells responded at light onset with action potentials (Figure 4D). To further determine whether the rabies-virus-labeled RGCs belong to M4-type mRGCs, we conducted disynaptic tracing in Opn4-Cre mice, in which mRGCs (including M4-type mRGCs) express Cre recombinase (Milosavljevic et al., 2016; Wang et al., 2017b). We observed that ~76.4% of rabies-virus-labeled RGCs were co-labeled with mRGCs expressing EYFP (Figure 4F), suggesting that M4-type mRGCs can form disynaptic connections with the LHb through the vLGN/IGL.

Activation of the vLGN/IGL-Projecting RGCs Decreases Depressive-like Behaviors

Given that axon terminals of RGCs release the excitatory neurotransmitter glutamate (Finlayson and Iezzi, 2010), and in view of our finding that activation of the vLGN/IGL-LHb pathway decreased depressive-like behaviors, we tested the effects of specific activation of the vLGN/IGL-projecting RGCs in a depressive-like mouse model induced by long-term exposure to AS. To determine whether the activation of the vLGN/IGL-projecting RGCs could prevent AS-induced depressive symptoms, we chemogenetically activated the vLGN/IGL-projecting RGCs expressing hM3D-mCherry during the last 14 days of exposure to AS (Figures 5A–5C). We found that specific activation of vLGN/IGL-projecting RGCs prevented the development of depressive symptoms (Figure 5C). To test whether activation of vLGN/IGL-projecting RGCs could reverse AS-induced depressive symptoms, we conducted 10 days of daily chemogenetic activation of the vLGN/IGL-projecting RGCs expressing hM3D-mCherry after exposing the mice to 28 days of AS (Figure 5D). Chemogenetic activation of the vLGN/IGL-projecting RGCs also reversed depressive-like behaviors (Figure 5D).

The Antidepressive Effect of Light Therapy Requires Activation of the Retina-vLGN/IGL-LHb Pathway

The above observations demonstrate that LHb-projecting vLGN/IGL neurons received M4-type mRGC input and that their activity inhibited LHb and suppressed depressive-like behaviors. We hypothesized that increased light detected by vLGN/IGL-projecting RGCs could inhibit neural activity in the LHb and ameliorate depressive symptoms through LHb-projecting vLGN/IGL neurons. To test this hypothesis, we first tested whether exposure to bright light attenuates the activation of LHb excitatory neurons through recording the Ca^{2+} signals in LHb CaMKIIa neurons expressing GCaMP6m with fiber photometry. We found that exposure to bright light (3,000 lux) impaired AS-induced activation of LHb excitatory neurons (Figures 6A and S9A), indicating that LHb neurons encoding AS can be inhibited by visual light stimulation. Next, we evaluated the efficacy of bright light therapy in a depressive-like mouse model induced by exposure to 28 days of AS. During the last 14 days of exposure to AS, animals received 2 h of daily light therapy of various intensities (70 lux, 600 lux, 2,000 lux, 3,000 lux, or 5,000 lux) (Figure 6B). We found that light therapy prevented the development of depressive symptoms and reduced the excitability and burst firing of LHb neurons in an intensity-dependent manner (Figures 6C–6E and S9B). Furthermore, light therapy (3,000 lux, 2 h/day) also reversed depressive symptoms induced by long-term exposure to AS or CSDS (Figures S10A and S10B). In contrast, light therapy did not decrease anxiety-like behaviors induced by long-term exposure to AS or CSDS (Figures S9C–S10A, and S10B), probably due to the excitatory effects of light exposure on anxiety-related brain regions, such as the amygdala (Figures S10C and S10D) (Milosavljevic et al., 2016).

To evaluate the role of the vLGN/IGL-LHb pathway in light therapy, we expressed Cre recombinase in LHb-projecting vLGN/IGL neurons by injection of rAAV2/2-Retro-Cre into the bilateral LHb and infected LHb-projecting vLGN/IGL neurons with AAV2/9-DIO-hM4D-mCherry (Figure 7B). LHb-projecting vLGN/IGL neurons were chemogenetically inhibited during light therapy (3,000 lux, 2 h/day) (Figures 7A, S11A, and S12A). Inhibition of LHb-projecting vLGN/IGL neurons abolished the antidepressive effects of light therapy in mice that received long-term exposure to AS or CSDS (Figures 7C, S11A, and S12B). To further determine whether the vLGN/IGL-LHb pathway is required for light treatment of depressive symptoms, we injected AAV2/1-Cre into the bilateral vLGN/IGL and infected postsynaptic LHb neurons with AAV2/9-DIO-hM3D-mCherry (Figure 7D). LHb postsynaptic neurons were chemogenetically activated during light therapy (Figures 7A, S11B, and S12A). We found that chemogenetic activation of LHb postsynaptic neurons also abolished the antidepressive effects of light therapy (Figures 7E, S11B, and S12C). Finally, we asked whether vLGN/IGL-projecting RGCs were required for light treatment of depressive symptoms by inhibiting vLGN/IGL-projecting RGCs during light therapy. To specifically inhibit vLGN/IGL-projecting RGCs, we delivered rAAV2/2-Retro-Cre into the bilateral vLGN/IGL and infected vLGN/IGL-projecting RGCs with AAV2/9-DIO-hM4D-mCherry through intraocular injection (Figure 7F). vLGN/IGL-projecting RGCs were chemogenetically inhibited during light therapy (Figures 7A, S11C, and S12A). Inhibition of vLGN/IGL-projecting RGCs eliminated the antidepressive effects of light therapy (Figures 7G, S11C, and S12D). Thus, activation of vLGN/IGL-projecting RGCs and of the vLGN/IGL-LHb pathway is required for bright light treatment of depressive symptoms evoked by long-term exposure to AS or CSDS.

DISCUSSION

Light therapy represents a cost-effective treatment for a variety of depressive conditions. Although a growing body of

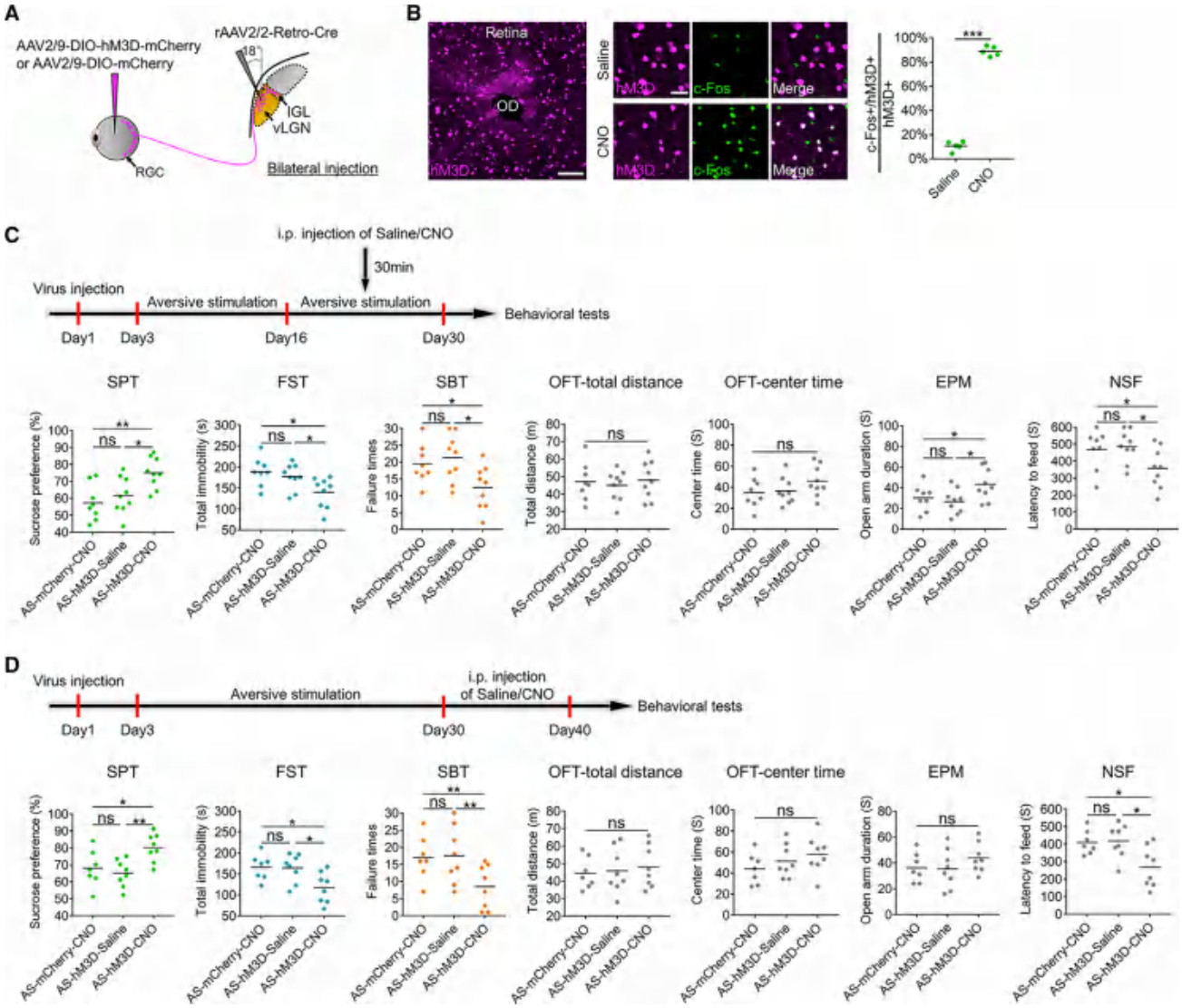

Figure 5. Activation of vLGN/IGL-Projecting RGCs Decreases Depressive-like Behaviors Induced by Long-Term Exposure to AS

(A) Scheme for specific infection of vLGN/IGL-projecting RGCs with hM3D or mCherry.

(B) Left: representative images of the retina showing i.p injection of saline or CNO evoked c-Fos expression in vLGN/IGL-projecting RGCs expressing hM3D. Right: percentage of total hM3D RGCs expressing c-Fos in different groups (n = 5 animals/group).

(C) Top: schematic of the experimental design. Bottom: depressive- and anxiety-like behaviors in different experimental groups (n = 8–9 animals/group). All mice received vLGN/IGL injection of rAAV2/2-Retro-Cre and exposure to AS. AS-mCherry-CNO, mice that received intraocular injection of AAV2/9-DIO-mCherry and i.p. injection of CNO; AS-hM3D-Saline, mice that received intraocular injection of AAV2/9-DIO-hM3D-mCherry and i.p. injection of saline; AS-hM3D-CNO, mice that received intraocular injection of AAV2/9-DIO-hM3D-mCherry and i.p. injection of CNO.

(D) Top: schematic of the experimental design. Bottom: depressive- and anxiety-like behaviors in different experimental groups (n = 7–8 animals/group). All mice received vLGN/IGL injection of rAAV2/2-Retro-Cre and exposure to AS. AS-mCherry-CNO, mice that received intraocular injection of AAV2/9-DIO-mCherry and i.p. injection of CNO; AS-hM3D-Saline, mice that received intraocular injection of AAV2/9-DIO-hM3D-mCherry and i.p. injection of saline; AS-hM3D-CNO, mice that received intraocular injection of AAV2/9-DIO-hM3D-mCherry and i.p. injection of CNO.

Scale bars represent 100 mm (B, left) and 50 mm (B, middle). For all figures, *p < 0.05, **p < 0.001, ***p < 0.0001, and ns, no significant difference (one-way ANOVA with Sidak's multiple comparisons test). Dot plots include horizontal lines indicating the mean.

research supports the efficacy of light therapy for individuals with both seasonal and nonseasonal depression (Rosenthal et al., 1984; Kripke, 1998; Golden et al., 2005; Wirz-Justice et al., 2009, 2011; Lieverse et al., 2011; Lam et al., 2016; Sit et al., 2018), there remain many unresolved questions regarding how light therapy produces its beneficial effects. The present study offers several lines of evidence demonstrating that the retina, vLGN/IGL and LHb are crucial elements of the neural circuitry for the antidepressive effects of light therapy.

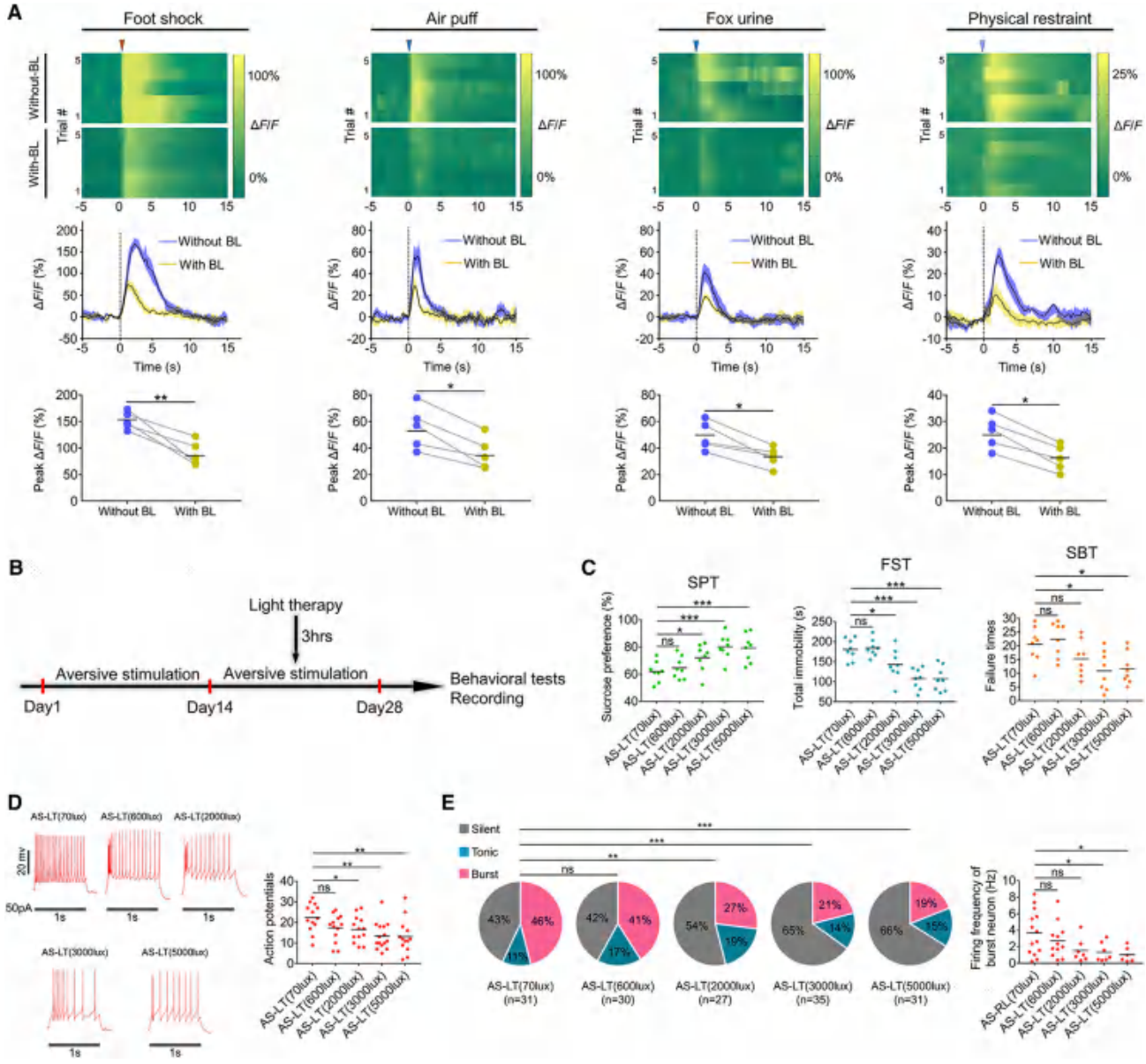

Figure 6. Light Therapy Decreases Depressive-like Behaviors Induced by Long-Term Exposure to AS

(A) Top (without-BL): heatmaps showing the Ca^{2+} signals evoked by AS in LHb CaMKIIa neurons from a C57BL/6 mouse exposed to room light (120 lux). Top (with-BL): heatmaps showing the Ca^{2+} signals in LHb CaMKIIa neurons from the same mouse used in the without-BL group, which received exposure to bright light (BL; 3,000 lux). Middle: averaged responses of mice in different groups. Bottom: Exposure to bright light significantly reduced the amplitude of Ca^{2+} signals associated with exposure to AS (n = 5 animals/group).

(B) Schematic of the experimental design.

(C) Depressive-like behaviors in mice received exposure to AS and different intensity of light therapy (LT; n = 8 animals/group).

(D) The current-evoked action potentials in brain slices of mice received exposure to AS and different intensities of LT (n = 13–15 cells/group).

(E) Left: pie charts indicate percentage of the three types of LHb neurons in mice received exposure to AS and different intensities of LT (n = 27–35 cells/group). Right: spontaneous firing frequency of burst neuron recorded with whole-cell current clamp (n = 6–14 cells/group).

For all figures, *p < 0.05, **p < 0.001, ***p < 0.0001, and ns, no significant difference (one-way ANOVA with Sidak's multiple comparisons test [A, C, D, and E, right] and chi-square test [E, left]). Dot plots include horizontal lines indicating the mean. See also Figures S9 and S10.

The visual thalamus to habenula projection has been proposed in numerous species, including lizard, frog, mouse, rat, rabbit, and human (Oh et al., 2014; Díaz and Puelles, 1992; Kemali et al., 1980; Moore et al., 2000; Cragg, 1961; Marburg, 1944; Ely et al., 2016; Torrisi et al., 2017). With a combination of retrograde and anterograde viral transsynaptic labeling techniques, we provide direct evidence that a subset of mouse vLGN/IGL GABA neurons can directly innervate LHb CaMKIIa

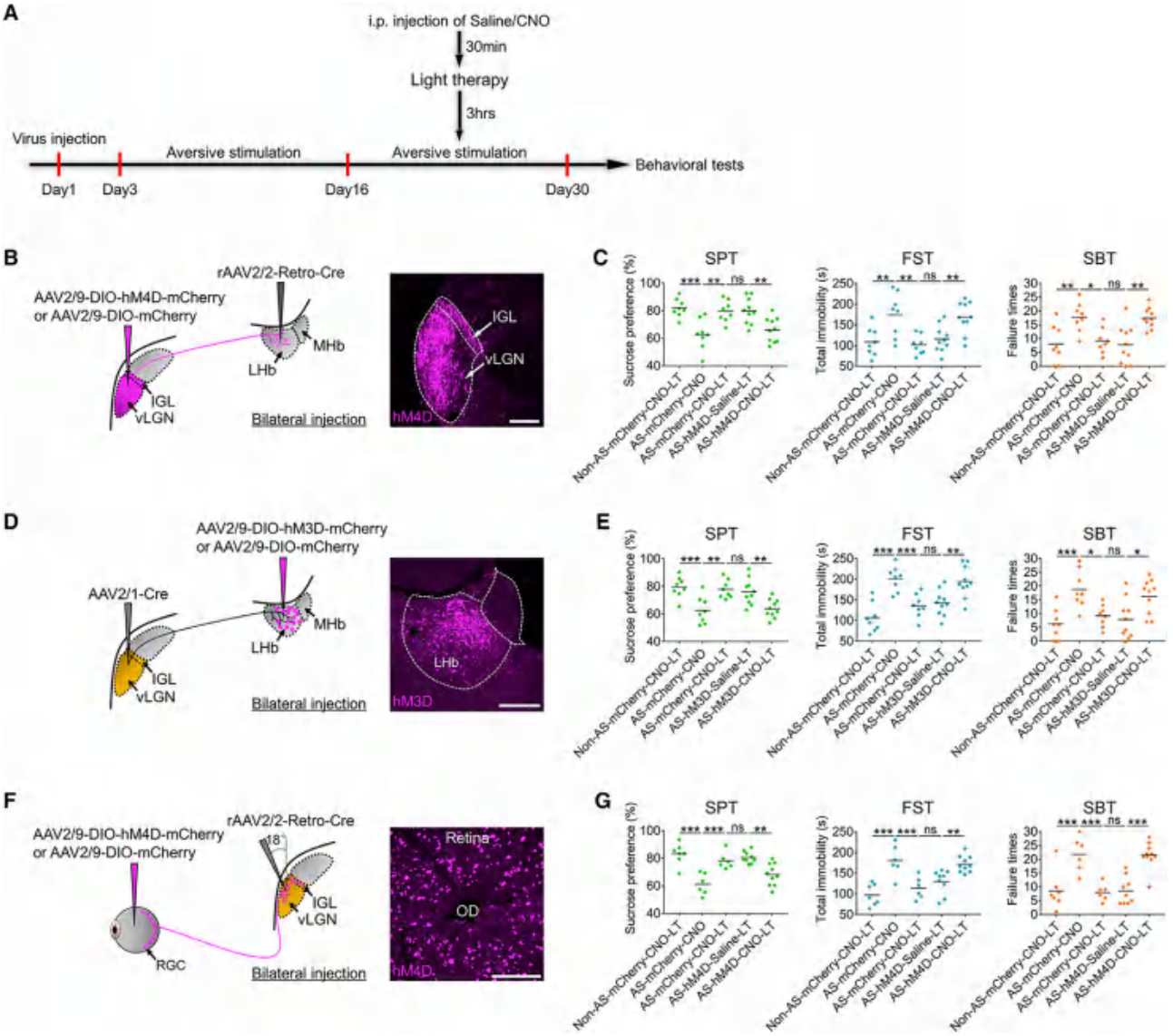

Figure 7. Activation of the Retina-vLGN/IGL-LHb Pathway Is Required for the Antidepressive Effects of Light Therapy

(A) Schematic of the experimental design.

(B) Scheme for specific infection of LHb-projecting vLGN/IGL neurons with hM4D or mCherry.

(C) Depressive-like behaviors in different experimental groups (n = 8–10 animals/group). All mice received LHb injection of rAAV2/2-Retro-Cre. Non-AS-mCherry-CNO-LT, mice that received vLGN/IGL injection of AAV2/9-DIO-mCherry, i.p. injection of CNO, LT (3,000 lux, 2 h/day), and no exposure to AS; AS-mCherry-CNO, mice that received vLGN/IGL injection of AAV2/9-DIO-mCherry, i.p. injection of CNO, and exposure to AS; AS-mCherry-CNO-LT, mice that received vLGN/IGL injection of AAV2/9-DIO-mCherry, i.p. injection of CNO, LT, and exposure to AS; AS-hM4D-Saline-LT, mice that received vLGN/IGL injection of AAV2/9-DIO-hM4D-mCherry, i.p. injection of saline, LT, and exposure to AS; AS-hM4D-CNO-LT, mice that received vLGN/IGL injection of AAV2/9-DIO-hM4D-mCherry, i.p. injection of CNO, LT, and exposure to AS.

(D) Scheme for specific infection of LHb postsynaptic neurons with hM3D or mCherry.

(E) Depressive-like behaviors in different experimental groups (n = 8–10 animals/group). All mice received vLGN/IGL injection of AAV2/1-Cre. Non-AS-mCherry-CNO-LT, mice that received LHb injection of AAV2/9-DIO-mCherry, i.p. injection of CNO, LT, and no exposure to AS; AS-mCherry-CNO, mice that received LHb injection of AAV2/9-DIO-mCherry, i.p. injection of CNO, and exposure to AS; AS-mCherry-CNO-LT: mice that received LHb injection of AAV2/9-DIO-mCherry, i.p. injection of CNO, LT, and exposure to AS; AS-hM3D-Saline-LT, mice that received LHb injection of AAV2/9-DIO-hM3D-mCherry, i.p. injection of saline, LT, and exposure to AS; AS-hM3D-CNO-LT, mice that received LHb injection of AAV2/9-DIO-hM3D-mCherry, i.p. injection of CNO, LT, and exposure to AS.

(F) Scheme for specific infection of vLGN/IGL-projecting RGCs with hM4D or mCherry.

(G) Depressive-like behaviors in different experimental groups (n = 6–10 animals/group). All mice received vLGN/IGL injection of rAAV2/2-Retro-Cre. Non-AS-mCherry-CNO-LT, mice that received intraocular injection of AAV2/9-DIO-mCherry, i.p. injection of CNO, LT, and no exposure to AS; AS-mCherry-CNO, mice that received intraocular injection of AAV2/9-DIO-mCherry, i.p. injection of CNO, and exposure to AS; AS-mCherry-CNO-LT, mice that received intraocular injection of AAV2/9-DIO-mCherry, i.p. injection of CNO, LT, and exposure to AS; AS-hM4D-Saline-LT, mice that received intraocular injection of

(legend continued on next page)

neurons. Furthermore, we demonstrate that selective activation of LHb-projecting vLGN/IGL neurons inhibits LHb neurons and impairs the excitatory effects of AS on the LHb. It is well documented that LHb aberrant hyperactivity is associated with an increase in depressive-like behaviors (Li et al., 2013; Lecca et al., 2016; Lawson et al., 2017; Boulos et al., 2017; Yang et al., 2018). It is therefore reasonable to postulate that activation of the vLGN/IGL-LHb pathway would decrease depressive-like behaviors. This prediction was borne out by our experiments using chemogenetic methods to activate LHb-projecting vLGN/IGL neurons or inhibit LHb postsynaptic neurons in two independent depressive-like mouse models: long-term activation of LHb-projecting vLGN/IGL neurons or inhibition of LHb postsynaptic neurons significantly decreased depressive-like behaviors and reduced aberrant hyperactivity of LHb neurons induced by exposure to AS or CSDS.

Recent studies found that increased bursting of LHb neurons caused by hyperpolarization of the resting membrane potentials drives depression, which can be induced by elevated level of astrocytic Kir4.1 in the LHb (Yang et al., 2018; Cui et al., 2018). Consistent with these findings, we found that burst firing of LHb neurons was significantly increased in our depressive-like mice model, which was reduced by activation of the vLGN/IGL-LHb pathway through chemogenetic methods or light therapy. Given that most of the LHb-projecting vLGN/IGL neurons are GABAergic, our results suggest that enhanced GABAergic synaptic inputs can reduce burst firing in the LHb. This is consistent with previous finding that burst generation in the LHb can be modulated by network synaptic inputs (Yang et al., 2018). Although LHb neurons may produce rebound bursts from inhibition (Weiss and Veh, 2011; Yang et al., 2018), we did not observe increased depressive-like behaviors in animals that received light therapy and no exposure to AS (Figures 7C, 7E, and 7G). Combining this result with our finding that chemogenetic activation of the vLGN/IGL-LHb pathway or light therapy significantly decreased depressive-like behaviors and reduced burst firing in the LHb, it is highly possible that even if chemogenetic activation of the vLGN/IGL-LHb pathway or light therapy generated rebound bursts in the LHb, the depression-inducing effects evoked by rebound bursts were weak and could be overridden by the antidepressive effects caused by the reduction of overall burst firing in the LHb.

Our virus-tracing data indicate that LHb postsynaptic neurons project to the DRN and VTA, which are implicated in the regulation of a broad range of mood-related behaviors, including reward-related behaviors, despair-like behaviors, and anxiety-like behaviors (Manji et al., 2001; Nestler et al., 2002; Yadid and Friedman, 2008; Lowry et al., 2008). This suggests that the manipulation of the vLGN/IGL-LHb pathway can produce effects on not only depressive-like behaviors but also other mood-related behaviors. Our data support this proposal, revealing that activation of the vLGN/IGL-LHb pathway also decreased anxiety-like behaviors induced by long-term exposure to AS or CSDS. These results are strongly consistent with previous findings that optogenetic inhibition or lesion of the LHb blocked the typical anxiety-like behaviors induced by exposure to inescapable tail shock or chronic stress (Dolzani et al., 2016; Jacinto et al., 2017).

It is well established that mRGCs play a crucial role in the modulation of non-image-forming visual functions such as cognition, circadian rhythms, and affective behaviors (LeGates et al., 2014). Six (M1–M6) and four (M1–M4) subtypes of mRGCs have been identified in rodents and humans, respectively (Ecker et al., 2010; Reifler et al., 2015; Hannibal et al., 2017; Quattrochi et al., 2019). Here, we found that M4-type mRGCs can directly innervate LHb-projecting vLGN/IGL neurons. As axon terminals of RGCs release the excitatory neurotransmitter glutamate (Finlayson and Iezzi, 2010), it is plausible that information about increased light transmitted by vLGN/IGL-projecting RGCs could alleviate depressive-like behaviors through the activation of the vLGN/IGL-LHb pathway. In support of this hypothesis, we demonstrate that either the inhibition of LHb-projecting vLGN/IGL neurons or the activation of LHb postsynaptic neurons abolishes the antidepressive effects of light therapy.

A recent study found that a subset of mRGCs (predominantly M1) in mice directly innervates the perihabenular nucleus (pHb), a previously unrecognized structure of the dorsal thalamus, which unlike the LHb of the epithalamus can be activated by dark-light transitions, but not by exposure to AS (Fernandez et al., 2018). The authors further demonstrated that chronic activation of the pHb by exposure to an ultradian light:dark cycle (T7 cycle; alternating 3.5-h periods of light and darkness) increased depressive-like behaviors (Fernandez et al., 2018). In view of our finding that light therapy decreased the depressive-like behaviors induced by exposure to AS or CSDS through the inhibition of LHb, it appears that even if both vLGN/IGL-projecting M4-type mRGCs and pHb-projecting mRGCs were activated during daily light therapy in our depressive-like mice model, the depression-inducing effects caused by the activation of the retina-pHb pathway were negated by the antidepressive effects induced by the activation of the retina-vLGN/IGL-LHb pathway. It is also important to note that the LHb was not activated by the dark-light transition (Figures S10C and S10D). It is therefore plausible that even if both the pHb-projecting mRGCs and M4-type mRGCs were activated during the T7 cycle, the antidepressive effects induced by activation of the retina-vLGN/IGL-LHb pathway were overridden by the depression-inducing effects caused by the chronic or repeated activation of the retina-pHb pathway.

In contrast to chemogenetic activation of the vLGN/IGL-LHb pathway, light therapy decreased only depressive-like behaviors and tended to increase anxiety-like behaviors, which are accompanied by the activation of the amygdala (Figures S9C and S10–S12). These results are similar to a recent finding that short-term activation of mRGCs (including M4-type and non-M4-type mRGCs) tended to decrease depressive-like behaviors but increased anxiety-like behaviors and c-Fos expression in the

AAV2/9-DIO-hM4D-mCherry, i.p. injection of saline, LT, and exposure to AS; AS-hM4D-CNO-LT, mice that received intraocular injection of AAV2/9-DIO-hM4D-mCherry, i.p. injection of CNO, LT, and exposure to AS.

Scale bars represent 200 ㎜ (B, D, and F). For all figures, *p < 0.05, **p < 0.001, ***p < 0.0001, and ns, no significant difference (one-way ANOVA with Sidak's multiple comparisons test). Dot plots include horizontal lines indicating the mean. See also Figures S11 and S12.

amygdala (Milosavljevic et al., 2016). The authors further demonstrated that short-term exposure to bright light also increased anxiety-like behaviors, and the anxiogenic effect of exposure to bright light was absent in mice lacking melanopsin (Milosavljevic et al., 2016). Since M4-type mRGCs express melanopsin at very low levels and exhibit a weak intrinsic light response (Estevez et al., 2012), it is plausible that the anxiogenic effects of exposure to bright light were mainly mediated by non-M4-type mRGCs. Combined with our data that activation of the vLGN/IGL-LHb pathway decreases anxiety-like behaviors, it appears that both M4-type and non-M4-type mRGCs are activated during light therapy and that the anxiolytic effects induced by the activation of M4-type mRGCs are suppressed by the anxiogenic effects induced by the activation of non-M4-type mRGCs.

Taken together, our results provide compelling evidence that light therapy can alleviate depressive-like behaviors through a dedicated subcortical neural circuit between the retina and LHb. Given the high conservation of mRGCs and visual thalamus to habenula projection in rodents and humans, these novel results may shed light on our current understanding of the mechanisms of light therapy.

STAR + METHODS

Detailed methods are provided in the online version of this paper and include the following:

- KEY RESOURCES TABLE
- CONTACT FOR REAGENT AND RESOURCE SHARING
- EXPERIMENTAL MODEL AND SUBJECT DETAILS
- METHOD DETAILS
  - Surgery and intracranial injection
  - Injection site verification
  - Physiological recording from brain slices
  - Fiber Photometry
  - Immunocytochemistry
  - Image analysis
  - Behavioral paradigms
  - Chemogenetic manipulation
- QUANTIFICATION AND STATISTICAL ANALYSIS
  - Fiber photometry data analysis
  - Quantification of neurons infected with different viruses
  - Quantification of c-Fos immunostaining
  - Statistics

SUPPLEMENTAL INFORMATION

Supplemental Information includes 12 figures and can be found with this article online at https://doi.org/10.1016/j.neuron.2019.01.037.

ACKNOWLEDGMENTS

We thank Dr. Wenbiao Gan and Dr. Gary Pickard for critical comments on the manuscript and Dr. Hailan Hu and Dr. Yihui Cui for advice concerning the firing pattern of LHb neurons. C.R. is supported by the National Natural Science Foundation of China (31771170 and 31400942), the National Program on Key Basic Research Project of China (973 Program, 2014CB542205), the Guangdong Special Support Program (2017TQ04R173), the Guangdong Natural Science Foundation (2014A030313387), the Pearl River S&T Nova Program of Guangzhou (201806010198), and Shenzhen Basic Research Grant JCYJ20170412164259361. M.P. is supported by the National Natural Science Foundation of China (31571091) and the National Program on Key Basic Research Project of China (973 Program, 2015CB351806). K.-F.S. is supported by funding from Leading Talents of Guangdong (2013) and the Programme of Introducing Talents of Discipline to Universities (B14036).

AUTHOR CONTRIBUTIONS

C.R. designed experiments and wrote the manuscript. L.H., Y.X., Y.P., Y.Y., and X.H. performed surgery. L.H., Y.X., Y.P., and Y.Y. performed behavioral experiments and in vivo activity recordings. X.H. and K.S. performed physiological recordings. Y.F., Q.T., and J.X. assisted with behavioral experiments, histology, and microscopy. C.R., K.-F.S., L.H., Y.X., X.H., and T.Y. analyzed the data. K.A., H.Z., M.P., F.X., T.X., and M.L. assisted with the analysis of virus tracing data.

DECLARATION OF INTERESTS

The authors declare no competing interests.

Received: August 30, 2018
Revised: December 18, 2018
Accepted: January 17, 2019
Published: February 19, 2019

REFERENCES

Aizawa, H., Kobayashi, M., Tanaka, S., Fukai, T., and Okamoto, H. (2012). Molecular characterization of the subnuclei in rat habenula. J. Comp. Neurol. 520, 4051–4066.

Berton, O., McClung, C.A., Dileone, R.J., Krishnan, V., Renthal, W., Russo, S.J., Graham, D., Tsankova, N.M., Bolanos, C.A., Rios, M., et al. (2006). Essential role of BDNF in the mesolimbic dopamine pathway in social defeat stress. Science 311, 864–868.

Boulos, L.J., Darcq, E., and Kieffer, B.L. (2017). Translating the habenula—from rodents to humans. Biol. Psychiatry 81, 296–305.

Cragg, B.G. (1961). The connections of the habenula in the rabbit. Exp. Neurol. 3, 388–409.

Cruz-Martín, A., El-Danaf, R.N., Osakada, F., Sriram, B., Dhande, O.S., Nguyen, P.L., Callaway, E.M., Ghosh, A., and Huberman, A.D. (2014). A dedicated circuit links direction-selective retinal ganglion cells to the primary visual cortex. Nature 507, 358–361.

Cui, Y., Yang, Y., Ni, Z., Dong, Y., Cai, G., Foncelle, A., Ma, S., Sang, K., Tang, S., Li, Y., et al. (2018). Astroglial Kir4.1 in the lateral habenula drives neuronal bursts in depression. Nature 554, 323–327.

Diaz, C., and Puelles, L. (1992). Afferent connections of the habenular complex in the lizard Gallotia galloti. Brain Behav. Evol. 39, 312–324.

Dolzani, S.D., Baratta, M.V., Amat, J., Agster, K.L., Saddoris, M.P., Watkins, L.R., and Maier, S.F. (2016). Activation of a habenulo-raphe circuit is critical for the behavioral and neurochemical consequences of uncontrollable stress in the male rat. eNeuro 3, ENEURO.0229-16.2016.

Ecker, J.L., Dumitrescu, O.N., Wong, K.Y., Alam, N.M., Chen, S.K., LeGates, T., Renna, J.M., Prusky, G.T., Berson, D.M., and Hattar, S. (2010). Melanopsin-expressing retinal ganglion-cell photoreceptors: cellular diversity and role in pattern vision. Neuron 67, 49–60.

Ely, B.A., Xu, J., Goodman, W.K., Lapidus, K.A., Gabbay, V., and Stern, E.R. (2016). Resting-state functional connectivity of the human habenula in healthy individuals: associations with subclinical depression. Hum. Brain Mapp. 37, 2369–2384.

Estevez, M.E., Fogerson, P.M., Ilardi, M.C., Borghuis, B.G., Chan, E., Weng, S., Auferkorte, O.N., Demb, J.B., and Berson, D.M. (2012). Form and function of the M4 cell, an intrinsically photosensitive retinal ganglion cell type contributing to geniculocortical vision. J. Neurosci. 32, 13608–13620.

Fernandez, D.C., Fogerson, P.M., Lazzerini Ospri, L., Thomsen, M.B., Layne, R.M., Severin, D., Zhan, J., Singer, J.H., Kirkwood, A., Zhao, H., et al.

(2018). Light affects mood and learning through distinct retina-brain pathways. Cell 175, 71–84.e18.

Finlayson, P.G., and Iezzi, R. (2010). Glutamate stimulation of retinal ganglion cells in normal and s334ter-4 rat retinas: a candidate for a neurotransmitter-based retinal prosthesis. Invest. Ophthalmol. Vis. Sci. 51, 3619–3628.

Golden, R.N., Gaynes, B.N., Ekstrom, R.D., Hamer, R.M., Jacobsen, F.M., Suppes, T., Wisner, K.L., and Nemeroff, C.B. (2005). The efficacy of light therapy in the treatment of mood disorders: a review and meta-analysis of the evidence. Am. J. Psychiatry 162, 656–662.

Golden, S.A., Covington, H.E., 3rd, Berton, O., and Russo, S.J. (2011). A standardized protocol for repeated social defeat stress in mice. Nat. Protoc. 6, 1183–1191.

Gonzalez, M.M., and Aston-Jones, G. (2008). Light deprivation damages monoamine neurons and produces a depressive behavioral phenotype in rats. Proc. Natl. Acad. Sci. USA 105, 4898–4903.

Gunaydin, L.A., Grosenick, L., Finkelstein, J.C., Kauvar, I.V., Fenno, L.E., Adhikari, A., Lammel, S., Mirzabekov, J.J., Airan, R.D., Zalocusky, K.A., et al. (2014). Natural neural projection dynamics underlying social behavior. Cell 157, 1535–1551.

Hannibal, J., Christiansen, A.T., Heegaard, S., Fahrenkrug, J., and Kiilgaard, J.F. (2017). Melanopsin expressing human retinal ganglion cells: subtypes, distribution, and intraretinal connectivity. J. Comp. Neurol. 525, 1934–1961.

Harrington, M.E. (1997). The ventral lateral geniculate nucleus and the intergeniculate leaflet: interrelated structures in the visual and circadian systems. Neurosci. Biobehav. Rev. 21, 705–727.

Hikosaka, O., Sesack, S.R., Lecourtier, L., and Shepard, P.D. (2008). Habenula: crossroad between the basal ganglia and the limbic system. J. Neurosci. 28, 11825–11829.

Jacinto, L.R., Mata, R., Novais, A., Marques, F., and Sousa, N. (2017). The habenula as a critical node in chronic stress-related anxiety. Exp. Neurol. 289, 46–54.

Kemali, M., Guglielmotti, V., and Gioffré, D. (1980). Neuroanatomical identification of the frog habenular connections using peroxidase (HRP). Exp. Brain Res. 38, 341–347.

Kripke, D.F. (1998). Light treatment for nonseasonal depression: speed, efficacy, and combined treatment. J. Affect. Disord. 49, 109–117.

Lam, R.W., Levitt, A.J., Levitan, R.D., Michalak, E.E., Cheung, A.H., Morehouse, R., Ramasubbu, R., Yatham, L.N., and Tam, E.M. (2016). Efficacy of bright light treatment, fluoxetine, and the combination in patients with nonseasonal major depressive disorder: a randomized clinical trial. JAMA Psychiatry 73, 56–63.

Lau, B.W., Ren, C., Yang, J., Yan, S.W., Chang, R.C., Pu, M., and So, K.F. (2011). Light deprivation induces depression-like behavior and suppresses neurogenesis in diurnal mongolian gerbil (Meriones unguiculatus). Cell Transplant. 20, 871–881.

Lawson, R.P., Nord, C.L., Seymour, B., Thomas, D.L., Dayan, P., Pilling, S., and Roiser, J.P. (2017). Disrupted habenula function in major depression. Mol. Psychiatry 22, 202–208.

Lecca, S., Pelosi, A., Tchenio, A., Moutkine, I., Lujan, R., Hervé, D., and Mameli, M. (2016). Rescue of GABAB and GIRK function in the lateral habenula by protein phosphatase 2A inhibition ameliorates depression-like phenotypes in mice. Nat. Med. 22, 254–261.

LeGates, T.A., Fernandez, D.C., and Hattar, S. (2014). Light as a central modulator of circadian rhythms, sleep and affect. Nat. Rev. Neurosci. 15, 443–454.

Li, K., Zhou, T., Liao, L., Yang, Z., Wong, C., Henn, F., Malinow, R., Yates, J.R., 3rd, and Hu, H. (2013). bCaMKII in lateral habenula mediates core symptoms of depression. Science 341, 1016–1020.

Lieverse, R., Van Someren, E.J., Nielen, M.M., Uitdehaag, B.M., Smit, J.H., and Hoogendijk, W.J. (2011). Bright light treatment in elderly patients with nonseasonal major depressive disorder: a randomized placebo-controlled trial. Arch. Gen. Psychiatry 68, 61–70.

Lowry, C.A., Hale, M.W., Evans, A.K., Heerkens, J., Staub, D.R., Gasser, P.J., and Shekhar, A. (2008). Serotonergic systems, anxiety, and affective disorder: focus on the dorsomedial part of the dorsal raphe nucleus. Ann. N Y Acad. Sci. 1148, 86–94.

Manji, H.K., Drevets, W.C., and Charney, D.S. (2001). The cellular neurobiology of depression. Nat. Med. 7, 541–547.

Marburg, O. (1944). The structure and fiber connections of the human habenula. J. Comp. Neurol. 80, 211–233.

Matsumoto, M., and Hikosaka, O. (2007). Lateral habenula as a source of negative reward signals in dopamine neurons. Nature 447, 1111–1115.

Milosavljevic, N., Cehajic-Kapetanovic, J., Procyk, C.A., and Lucas, R.J. (2016). Chemogenetic activation of melanopsin retinal ganglion cells induces signatures of arousal and/or anxiety in mice. Curr. Biol. 26, 2358–2363.

Monje, F.J., Cabatic, M., Divisch, I., Kim, E.J., Herkner, K.R., Binder, B.R., and Pollak, D.D. (2011). Constant darkness induces IL-6-dependent depression-like behavior through the NF-kB signaling pathway. J. Neurosci. 31, 9075–9083.

Moore, R.Y., Weis, R., and Moga, M.M. (2000). Efferent projections of the intergeniculate leaflet and the ventral lateral geniculate nucleus in the rat. J. Comp. Neurol. 420, 398–418.

Nestler, E.J., Barrot, M., DiLeone, R.J., Eisch, A.J., Gold, S.J., and Monteggia, L.M. (2002). Neurobiology of depression. Neuron 34, 13–25.

Oh, S.W., Harris, J.A., Ng, L., Winslow, B., Cain, N., Mihalas, S., Wang, Q., Lau, C., Kuan, L., Henry, A.M., et al. (2014). A mesoscale connectome of the mouse brain. Nature 508, 207–214.

Proulx, C.D., Hikosaka, O., and Malinow, R. (2014). Reward processing by the lateral habenula in normal and depressive behaviors. Nat. Neurosci. 17, 1146–1152.

Pulmanausahakul, R., Li, J., Schnell, M.J., and Dietzschold, B. (2008). The glycoprotein and the matrix protein of rabies virus affect pathogenicity by regulating viral replication and facilitating cell-to-cell spread. J. Virol. 82, 2330–2338.

Quattrochi, L.E., Stabio, M.E., Kim, I., Ilardi, M.C., Michelle Fogerson, P., Leyrer, M.L., and Berson, D.M. (2019). The M6 cell: a small-field bistratified photosensitive retinal ganglion cell. J. Comp. Neurol. 527, 297–311.

Reifler, A.N., Chervenak, A.P., Dolikian, M.E., Benenati, B.A., Meyers, B.S., Demertzis, Z.D., Lynch, A.M., Li, B.Y., Wachter, R.D., Abufarha, F.S., et al. (2015). The rat retina has five types of ganglion-cell photoreceptors. Exp. Eye Res. 130, 17–28.

Rosenthal, N.E., Sack, D.A., Gillin, J.C., Lewy, A.J., Goodwin, F.K., Davenport, Y., Mueller, P.S., Newsome, D.A., and Wehr, T.A. (1984). Seasonal affective disorder. A description of the syndrome and preliminary findings with light therapy. Arch. Gen. Psychiatry 41, 72–80.

Sit, D.K., McGowan, J., Wiltrout, C., Diler, R.S., Dills, J.J., Luther, J., Yang, A., Ciolino, J.D., Seltman, H., Wisniewski, S.R., et al. (2018). Adjunctive bright light therapy for bipolar depression: a randomized double-blind placebo-controlled trial. Am. J. Psychiatry 175, 131–139.

Tervo, D.G., Hwang, B.Y., Viswanathan, S., Gaj, T., Lavzin, M., Ritola, K.D., Lindo, S., Michael, S., Kuleshova, E., Ojala, D., et al. (2016). A designer AAV variant permits efficient retrograde access to projection neurons. Neuron 92, 372–382.

Torrisi, S., Nord, C.L., Balderston, N.L., Roiser, J.P., Grillon, C., and Ernst, M. (2017). Resting state connectivity of the human habenula at ultra-high field. Neuroimage 147, 872–879.

Tovote, P., Esposito, M.S., Botta, P., Chaudun, F., Fadok, J.P., Markovic, M., Wolff, S.B., Ramakrishnan, C., Fenno, L., Deisseroth, K., et al. (2016). Midbrain circuits for defensive behaviour. Nature 534, 206–212.

Wang, D., Li, Y., Feng, Q., Guo, Q., Zhou, J., and Luo, M. (2017a). Learning shapes the aversion and reward responses of lateral habenula neurons. eLife 6, 6.

Wang, Q., Yue, W.W.S., Jiang, Z., Xue, T., Kang, S.H., Bergles, D.E., Mikoshiba, K., Offermanns, S., and Yau, K.W. (2017b). Synergistic signaling

by light and acetylcholine in mouse iris sphincter muscle. Curr. Biol. 27, 1791–1800.e5.

Weiss, T., and Veh, R.W. (2011). Morphological and electrophysiological characteristics of neurons within identified subnuclei of the lateral habenula in rat brain slices. Neuroscience 172, 74–93.

Wilson, N. (2002). Depression and its relation to light deprivation. Psychoanal. Rev. 89, 557–567.

Wirz-Justice, A., Benedetti, F., and Terman, M. (2009). Chronotherapeutics for Affective Disorders (Karger).

Wirz-Justice, A., Bader, A., Frisch, U., Stieglitz, R.D., Alder, J., Bitzer, J., Hösli, I., Jazbec, S., Benedetti, F., Terman, M., et al. (2011). A randomized, double-blind, placebo-controlled study of light therapy for antepartum depression. J. Clin. Psychiatry 72, 986–993.

Yadid, G., and Friedman, A. (2008). Dynamics of the dopaminergic system as a key component to the understanding of depression. Prog. Brain Res. 172, 265–286.

Yang, Y., Cui, Y., Sang, K., Dong, Y., Ni, Z., Ma, S., and Hu, H. (2018). Ketamine blocks bursting in the lateral habenula to rapidly relieve depression. Nature 554, 317–322.

Zhao, H., and Rusak, B. (2005). Circadian firing-rate rhythms and light responses of rat habenular nucleus neurons in vivo and in vitro. Neuroscience 132, 519–528.

Zingg, B., Chou, X.L., Zhang, Z.G., Mesik, L., Liang, F., Tao, H.W., and Zhang, L.I. (2017). AAV-mediated anterograde transsynaptic tagging: mapping corticocollicular input-defined neural pathways for defense behaviors. Neuron 93, 33–47.

STAR + METHODS

KEY RESOURCES TABLE

REAGENT or RESOURCE	SOURCE	IDENTIFIER
Antibodies		
Rabbit Anti-CaMKIIa	Abcam	Cat# ab5683; RRID: AB_305050
Streptavidin-Alexa Fluor 647	Thermo Fisher Scientific	Cat# S21374; RRID: AB_2336066
Rabbit Anti-c-Fos	Cell Signaling Technology	Cat# 2250; RRID: AB_2247211
Mouse Anti-SMI-32	BioLegend	Cat# 801703; RRID: AB_2626043
DyLight 594 Goat Anti-Rabbit	Vector Laboratories	Cat# DI-1594; RRID: AB_2336413
Alexa Fluor 488-conjugated Goat Anti-Rabbit	Jackson ImmunoResearch	Cat# 111-545-003; RRID: AB_2338046
DyLight 594 Goat Anti-Mouse	Thermo Fisher Scientific	Cat# 35510; RRID: AB_1185569
Bacterial and Virus Strains		
AAV2/9-Ef1a-DIO-eYFP	BrainVTA, Wuhan	Cat# PT-0012
AAV2/1-hSyn-Cre	BrainVTA, Wuhan	Cat# PT-0136
AAV2/9-Ef1a-DIO-hChR2(H134R)-eYFP	Taitool BioScience Co, Shanghai	Cat# S0199-9
AAV2/9-hSyn-DIO-mCherry	Taitool BioScience Co, Shanghai	Cat# S0240-9
AAV2/9-hSyn-DIO-hM3D(Gq)-mCherry	Taitool BioScience Co, Shanghai	Cat# S0192-9
AAV2/9-hSyn-DIO-hM4D(Gi)-mCherry	Taitool BioScience Co, Shanghai	Cat# S0193-9
rAAV2/2-hSyn-Retro-Cre	Taitool BioScience Co, Shanghai	Cat# S0278
AAV2/9-hSyn-DIO-tdTomato-T2A-Synaptophysin-eGFP	Taitool BioScience Co, Shanghai	Cat# S0161-9
AAV2/5-CaMKIIa-GCaMP6m	Taitool BioScience Co, Shanghai	Cat# S0481-5
AAV2/9-hSyn-EGFP-2a-TVA-2a-RVG-WPREs-pA	BrainVTA, Wuhan	Cat# PT-0022
Rabies virus SAD-DG-DsRed (EnvA)	BrainVTA, Wuhan	Cat# RV-306
Chemicals, Peptides, and Recombinant Proteins		
Clozapine N-oxide (CNO)	Sigma-Aldrich	Cat# C0832
Red Retrobeads	Lumafluor	Cat# R180
Green Retrobeads	Lumafluor	Cat# G180
Alexa Fluor 647-conjugated Cholera Toxin Subunit B	Thermo Fisher Scientific	Cat# C34778
4-Aminopyridine (4-AP)	Tocris	Cat# 0940
SR95531	Tocris	Cat# 1262
CNQX	Tocris	Cat# 0190
Tetrodotoxin (TTX)	Tocris	Cat# 1078
Experimental Models: Organisms/Strains		
Mouse: C57BL/6	Guangdong Medical Laboratory Animal Center, Guangzhou, China	N/A
Mouse: vGAT-Cre	The Jackson Laboratory	Tg(Slc32a1-Cre)2.1Hzo/FrkJ Stock No:017535
Mouse: Opn4-Cre	Wang et al., 2017b	N/A
Mouse: CD-1	Beijing Vital River Laboratory Animal Technology Co., Ltd. (China)	N/A
Software and Algorithms		
GraphPad Prism 7	GraphPad Software	N/A
ImageJ	NIH	https://imagej.nih.gov/ij
Excel	Microsoft	N/A
Photoshop CS5	Adobe	N/A
MATLAB 2014a and 2017a	MathWorks	N/A

(Continued on next page)

Continued

REAGENT or RESOURCE	SOURCE	IDENTIFIER
Other		
Fiber photometry system	Nanjing ThinkerTech	N/A
Optical fiber	Thorlabs	FT200UMT
Ceramic ferrule	Fiblaser Technology	N/A

CONTACT FOR REAGENT AND RESOURCE SHARING

Further information and request for resources and reagents should be directed to and will be fulfilled by the Lead Contact, Chaoran Ren (tchaoran@jnu.edu.cn).

EXPERIMENTAL MODEL AND SUBJECT DETAILS

All experiments were approved by the Jinan University Institutional Animal Care and Use Committee. Adult (6-8 weeks old) male C57BL/6 mice, vGAT-Cre [STOCK Tg(Slc32a1-cre)2.1Hzo/FrkJ] mice and Opn4-Cre mice (Wang et al., 2017b) were used in this study. Animals were housed under a 12 h:12 h light-dark cycle (lights on at 7 AM) with food and water provided ad libitum. Animals were randomly allocated to experimental and control groups. Experimenters were blind to the experimental group, and the order of testing was counterbalanced during behavioral experiments.

METHOD DETAILS

Surgery and intracranial injection

Mice were anaesthetized (Avertin, 13 ml/g, i.p.) and placed in a stereotaxic instrument. Erythromycin eye ointment was applied to prevent corneal drying and a heat pad was used to hold body temperature at 37°C. A small craniotomy hole was made using a dental drill (OmniDrill35, WPI, Sarasota, FL), and injections were performed via a micropipette connected to a Nanoliter Injector (NANOLITER 2010, WPI, Sarasota, FL) and its controller (Micro4, WPI, Sarasota, FL).

To specifically infect vLGN/IGL GABA neurons with mCherry, AAV2/9-hSyn-DIO-mCherry was injected into the vLGN/IGL of vGAT-Cre mice (virus titers: 3-5 3 10^{12} particles/ml, 0.2 ml/injection; AP: −2.2 mm; ML: ± 2.5 mm; DV: −3.2 mm). To retrogradely label LHb-projecting vLGN/IGL neurons with retrobeads, green retrobeads (Lumafluor, US, 0.05 ml/injection) was injected into the LHb of vGAT-Cre mice.

To specifically infect LHb-projecting vLGN/IGL neurons with ChR2-eYFP, mCherry, hM3D-mCherry or hM4D-mCherry, rAAV2/2-hSyn-Retro-Cre was injected into the LHb of C57BL/6 mice (virus titers: 2-4 3 10^{12} particles/ml; 0.1 ml/injection; AP: −1.6 mm; ML: ± 0.3 mm; DV: −3.05 mm), AAV2/9-Ef1a-DIO-hChR2(H134R)-eYFP, AAV2/9-hSyn-DIO-mCherry, AAV2/9-hSyn-DIO-hM3D(Gq)-mCherry or AAV2/9-hSyn-DIO-hM4D(Gi)-mCherry was injected into the vLGN/IGL (virus titers: 3-5 3 10^{12} particles/ml, 0.2 ml/injection).

To specifically infect postsynaptic LHb neurons with eYFP, tdTomato-T2A-Synaptophysin-eGFP, mCherry, hM3D-mCherry or hM4D-mCherry, AAV2/1-hSyn-Cre (virus titers: 3-5 3 10^{12} particles/ml; 0.15 ml/injection) and Alexa Fluor 647-conjugated Cholera Toxin Subunit B (CTB-647, 0.02 ml/injection, Invitrogen Inc., Grand Island, NY) were injected into the vLGN/IGL, and AAV2/9-Ef1a-DIO-eYFP, AAV2/9-hSyn-DIO-tdTomato-T2A-Synaptophysin-eGFP, AAV2/9-hSyn-DIO-mCherry, AAV2/9-hSyn-DIO-hM3D(Gq)-mCherry or AAV2/9-hSyn-DIO-hM4D(Gi)-mCherry was injected into the LHb (0.1 ml/injection). To retrogradely label DRN-projecting LHb neurons and VTA-projecting LHb neurons with retrobeads, red retrobeads was injected into the DRN and the VTA, respectively (Lumafluor, US, 0.1 ml/injection).

To infect LHb CaMKIIa neurons with GCaMP6m, AAV2/5-CaMKIIa-GCaMP6m was injected into the LHb (virus titers: 4.35 3 10^{12} particles/ml, 0.1 ml/injection).

To specifically infect vLGN/IGL-projecting RGCs with mCherry, hM3D-mCherry or hM4D-mCherry, rAAV2/2-hSyn-Retro-Cre was injected into the bilateral vLGN/IGL of C57BL/6 mice (0.1 ml/injection), AAV2/9-hSyn-DIO-mCherry, AAV2/9-hSyn-DIO-hM3D(Gq)-mCherry or AAV2/9-hSyn-DIO-hM4D(Gi)-mCherry was injected intraocularly (1.5 ml/eye).

For di-synaptic tracing of the retina / vLGN/IGL / LHb pathway, 0.2 mL Helper virus (AAV2/9-hSyn-EGFP-2a-TVA-2a-RVG-WPREs-pA) (virus titers: 2 3 10^{8} particles/ml) was injected into the vLGN/IGL (10 C57BL/6 mice and 11 Opn4-Cre mice). The pipette was held in place for 10 min, and then withdrawn slowly. Twenty-one days later, 0.1 mL of SAD-DG-DsRed (EnvA) (virus titers: 2 3 10^{8} particles/ml) was injected into the LHb.

To specifically infect mRGCs of Opn4-Cre mice with eYFP, AAV2/9-Ef1a-DIO-eYFP was injected intraocularly (1.5 ml/eye).

Following injection, the wound was sutured, antibiotics (bacitracin and neomycin) were applied to the surgical wound and ketoprofen (5 mg/kg) was injected subcutaneously; animals were allowed to recover from anesthesia under a heat lamp.

Injection site verification

After transcardial perfusion with 0.9% saline followed by 4% paraformaldehyde in 0.1 M phosphate-buffered saline (PBS), the brain was removed and post-fixed with 4% paraformaldehyde overnight at 4°C, and then transferred into 30% sucrose until sectioning with a cryostat (CM1900, Leica Microsystems, Bannockburn, IL). A series of 40 mm sections was collected for verification of injection sites. Tissue sections were examined under epifluorescence using a Zeiss Axioimager Z2 microscope.

Physiological recording from brain slices

For brain slice preparation, mice were deeply anaesthetized with isoflurane and coronal sections (250 mm thick) across the LHb were cut under ice-cold artificial cerebrospinal fluid (ACSF, in mM: 119 NaCl; 2.5 KCl, 1 NaH_2PO_4, 11 glucose, 26.2 $NaHCO_3$, 2.5 $CaCl_2$, and 1.3 $MgCl_2$, at pH 7.4, 290 mOsm) using a vibratome (VT1200S; Leica Microsystems). The brain slices were recovered for ~1 h at room temperature in ACSF. After recovery, slices were placed in the recording chamber and continuously perfused with ACSF.

Evoked postsynaptic currents were elicited by 1 ms blue light stimulation of axon terminals of LHb-projecting vLGN/IGL neurons infected with ChR2. Blue-light-evoked postsynaptic currents were recorded with Cs^+-based peptide solution (in mM: 130 $CsMeSO_4$, 10 NaCl, 10 EGTA, 4 MgATP, 0.3 Na_3GTP, 10 HEPES, 290 mOsm, adjust to 7.4 with CsOH). EPSCs and IPSCs were recorded when the membrane potential was holding at −70 mV and 0 mV, respectively. To test whether the recorded IPSCs were mediated by $GABA_A$ receptors, 100 mM SR95531 was added to the ACSF. To test whether the recorded EPSCs were mediated by AMPA/kainate receptors, 10 mM CNQX was added to the ACSF. To test whether the postsynaptic currents recorded in LHb neurons were elicited by direct synaptic connections, 1 mM tetrodotoxin (TTX) and 100 mM 4-aminopyridine (4-AP) were added to the ACSF. The recorded cells were intracellularly filled with biocytin for morphological evaluation.

To measure the excitability of LHb neurons, electrodes were filled with a K^+-based solution containing (in mM) 135 $KMeSO_4$, 10 KCl, 10 HEPES, 10 Na_2-phosphocreatine, 4 MgATP, 0.3 Na_3GTP, 290 mOsm, adjust to 7.4 with KOH. Depolarizing currents were applied (1 s for 50 pA and 0.15 s for 100 pA) from a membrane potential of −70 mV. Spontaneous firing was recorded with ACSF in the electrodes.

To determine the firing pattern of LHb neurons, the spontaneous neuronal activity was recorded under current-clamp at resting conditions (I = 0 pA). LHb neurons were classified as silent, tonic or burst based on spontaneous patterns of firing (Yang et al., 2018).

All recordings were performed using a Multiclamp 700B amplifier (Molecular Devices). Traces were low-pass filtered at 2 kHz and digitized at 10 kHz. For light stimulation, light pulses were delivered through digital commands from the Digidata 1550A and Digital stimulator (PG4000a, Cygnus Technology). The pipette resistance was ranged from 4 to 6 MU. When stable whole-cell recordings were achieved with an access resistance below 25 MU, basic electrophysiological properties were recorded. Offline data analysis was performed using Clampfit 10.0 software (Molecular Devices).

Fiber Photometry

A fiber photometry system was used for recording Ca^{2+} signals from LHb CaMKIIa neurons. Briefly, one week after AAV2/5-CaMKIIa-GCaMP6m virus injection, an optical fiber [O.D. = 230 mm, numerical aperture (NA) = 0.37] was placed in a ceramic ferrule and inserted toward the LHb through the craniotomy (coordinates: AP: −1.6 mm; ML: ± 0.35 mm; DV: −2.6 mm). The ceramic ferrule was supported with a skull-penetrating M1 screw and dental acrylic. Mice were individually housed and allowed to recover for at least one week. To record fluorescence signals, the laser beam from a 488-nm laser (OBIS 488LS; Coherent) was reflected by a dichroic mirror (MD498; Thorlabs), focused by a 10 x objective lens (NA = 0.3; Olympus) and then coupled to an optical commutator (Doric Lenses). An optical fiber (O.D. = 230 mm, NA = 0.37, 2 m long) guided the light between the commutator and the implanted optical fiber. The laser power was adjusted at the tip of the optical fiber to a low level of 0.01 - 0.02 mW in order to minimize bleaching.

The GCaMP6m fluorescence was bandpass filtered (MF525-39, Thorlabs) and collected with a photomultiplier tube (R3896, Hamamatsu). An amplifier (C7319, Hamamatsu) was used to convert the photomultiplier tube current output to voltage signals, which were further filtered through a low-pass filter (40 Hz cut-off; Brownlee 440). The analog voltage signals were digitized at 500 Hz and recorded with a Power 1401 digitizer and Spike2 software (CED, Cambridge, UK).

During the recording of Ca^{2+} signals in mice that received the LHb injections of rAAV2/2-hSyn-Retro-Cre and vLGN/IGL injections of AAV2/9-hSyn-DIO-hM3D(Gq)-mCherry, CNO and saline recordings were performed in the same animals. Specifically, 24 mice were divided into 4 groups: foot shock (n = 6 animals), air puff (n = 6 animals), fox urine (n = 6 animals), and physical restraint (n = 6 animals). The mice in each group received an i.p. injection of CNO, followed by saline 24 h later.

To test whether exposure to bright light attenuates the activation of LHb excitatory neurons, we used fiber photometry to record the AS (foot shock, air puff, fox urine, physical restraint) evoked Ca^{2+} signals in LHb CaMKIIa neurons expressing GCaMP6m with/without exposure to bright light (3000 Lux). With and without exposure to bright light recordings were performed in the same animals. Specifically, AS-evoked Ca^{2+} signals were first recorded under bright light conditions (3000 lux). Twenty-four hours later, AS-evoked Ca^{2+} signals were recorded again under room light conditions (120 lux).

Immunocytochemistry

All animals were anaesthetized (Avertin, 13 ml/g, i.p.) and perfused intracardially with 0.9% saline followed by 4% paraformaldehyde in PBS. Brains and eyes were removed.

For CaMKIIa labeling, cryostat sections containing the LHb were placed in 0.1 M PBS containing 10% normal goat serum (Vector Laboratories, Burlingame, CA) and 0.3% Triton X-100 (T8787, Sigma-Aldrich, St Louis, MO) for 1 h before incubation in primary antibody against CaMKIIa (rabbit, 1:500; ab5683, Abcam) (36 h at 4°C). Sections were then incubated with the corresponding secondary antibody at a dilution of 1:400 for 6 h at room temperature: (DyLight 594) goat-anti-rabbit IgG (DI-1594, Vector Laboratories).

For detection of biocytin-filled LHb neurons, cryostat sections containing the LHb were placed in 0.1 M PBS containing 10% normal goat serum (Vector Laboratories, Burlingame, CA) and 0.3% Triton X-100 (T8787, Sigma-Aldrich, St Louis, MO) for 1 h before incubation in Streptavidin-Alexa Fluor 647 (1:100, S21374, Thermo Fisher Scientific) for 48 h at 4°C.

For c-Fos labeling, procedures used in CaMKIIa labeling were adopted except that the primary antibody was replaced with antibody against c-Fos (rabbit, 1:500, 2250, Cell Signaling Technology), and the secondary antibody was replaced with goat anti-rabbit Alexa Fluor 488 (1:400, 111-545-003, Jackson ImmunoResearch).

For detection of SMI-32-immunoreactive RGCs, retinas were isolated and washed in 0.1 M PBS 3 times (10 min each) before incubation in 0.1 M PBS containing 10% normal goat serum (Vector Laboratories, Burlingame, CA) and 0.3% Triton X-100 (T8787, Sigma-Aldrich, St Louis, MO) for 1 h. Then retinas were incubated for 3 days at 4°C with a mouse anti-SMI-32 antibody (1:1000, 801703, Biolegend). This was followed by 6 rinses in 0.1 M PBS and then incubation with a secondary (DyLight 594) goat-anti-mouse IgG (1:400, 35510, Thermo Fisher Scientific) for 6 h at room temperature.

Finally, all sections and retinas were rinsed in 0.1 M PBS and coverslipped in anti-fading aqueous mounting medium with DAPI (EMS, Hatfield, PA).

Image analysis

Retinas and sections were imaged with a Zeiss 700 confocal microscope with 5x or 20x objectives or a 40x oil immersion objective. For three-dimensional reconstruction of injected or virus-labeled cells, optical sections were collected at 0.2 mm intervals. Each stack of optical sections covered a retinal area of 325.75 3 325.75 mm^2 (1024 3 1024 pixels). Using ImageJ and Photoshop CS5 (Adobe Corp., San Jose, California, USA), each stack of optical sections was montaged and projected to a 0° X-Y plane and a 90° Y-Z plane to obtain a three-dimensional reconstruction of the cell. Contrast and brightness were adjusted, and the red-green images were converted to magenta-green. For each rabies virus-labeled RGC, the total sizes of the soma and dendritic field were analyzed. Dendritic field area was calculated by drawing a convex polygon linking the dendritic terminals. The dendritic field area was then calculated, and the diameter was calculated as that of a circle having an equal area.

Behavioral paradigms

All behavioral tests were conducted during the light phase (7 AM – 7 PM). Operators were blinded to the experimental group during the scoring.

Foot shock exposure

Mice were placed into an acrylic box (25 cm 3 25 cm 3 40 cm) equipped with a metal grid floor. To record foot shock evoked Ca^{2+} signals in LHb CaMKIIa neurons, foot shocks (1 mA, 500 ms) were delivered with inter-trial intervals of 15 s. Shock delivery onset was used as the trigger event for data alignment. To establish a depressive-like mouse model, foot shocks (20 times/day, 1 mA, 500 ms) were randomly delivered with inter-trial intervals of 15, 20 or 30 s. For the control group, mice were placed in the same acrylic box but did not receive foot shock stimulation.

Air puff exposure

To record air puff-evoked Ca^{2+} signals in LHb CaMKIIa neurons, the body of the mouse was inserted into an acrylic 'body tube', with the mouse's head extending out. A brief air puff was delivered to the face of the mouse by pressing a hand-pump air compressor (13 3 5 cm) attached to a PVC tube with its opening positioned ~5 cm away from the mouse's nostril. One press of the hand pump generates a ~2 s-long gentle air puff. Air puffs were delivered with inter-trial intervals of ~15 s. Onset of air puff delivery was used as the trigger event for data alignment. To establish a depressive-like mouse model, mice were placed in their home cages, and air puffs (20 times/day) were randomly delivered to the faces of the mice with inter-trial intervals of 10-15 s.

Fox urine exposure

To record fox urine-evoked Ca^{2+} signals in LHb CaMKIIa neurons, the body of the mouse was inserted into an acrylic 'body tube', with the head extending out. A cotton ball soaked with red fox urine (2 mL of Red fox P; Timk's, Safariland Hunting Corp., Trappe, MA) was placed ~1 cm away from the nostril of the mouse. To establish a depressive-like mouse model, mice were kept in a transparent plastic container (25 cm 3 10 cm 3 10 cm, with holes) containing 4 cotton balls soaked with red fox urine—for 30 min/day. For the control group, instead of fox urine, we added 2 mL of water.

Physical restraint

To record physical restraint-evoked Ca^{2+} signals in LHb CaMKIIa neurons, a well-trained experimenter restrained the mouse for ~5 s by placing gentle pressure on the mouse body with the left hand and immobilizing the tail with the right hand. To establish a depressive-like mouse model, the mice were restrained for 1 h/day in a plastic restrainer. After restraint treatment, the mice were returned to their own cages.

Bright light therapy

This experiment was started 1 h after the onset of the light phase and continued for 2 h (8 AM-10 AM). Mice were kept in their home cages which were placed in a custom-designed light therapy cabinet (30 cages/cabinet). Full spectrum bright light was supplied by cool LED lights (UV-free) and the intensity was determined by averaging the measurements from the top and the four sides of the cage. Following 14 days/10 days of treatment all animals underwent behavioral tests as detailed below.

Sucrose preference test (SPT)

Mice were tested for preference for a 2% sucrose solution (Sucrose, Sigma-Aldrich) using a two-bottle choice procedure. Each animal was housed individually during the 2-day test period. Animals were given two bottles, one of sucrose and one of tap water. Every 24 h, the amounts of sucrose and water consumed were recorded. To prevent potential location preference for drinking, the positions of the bottles were changed every 24 h. Food and water were available ad libitum prior to the SPT. The preference for the sucrose solution was determined as the percentage of sucrose solution ingested relative to the total intake.

Forced swimming test (FST)

Mice were placed in a cylinder of water (temperature of 23 – 25°C; 20 cm in diameter, 27 cm in height for mice) for 6 min. The depth of water was set to prevent animals from touching the bottom with their hind limbs. Animal behavior was video-tracked from the side. The time each animal spent immobile during the test was counted online by two independent observers in a blinded manner. Immobility was defined as no active movement except that needed to keep the animal from drowning.

Shuttle box test (SBT)

Mice were placed into a shuttle box (15 cm length 3 24 cm width 3 20 cm height) equipped with a metal grid floor and a door separating the two compartments. During the test, mice were administered 30 0.1-0.3 mA foot shocks for 10 s (30 s inter-trial interval). The foot shock terminated any time that the mice fled into the other compartment. Failure is defined as the absence of fleeing into the other compartment within the 10 s foot shock delivery.

Open field test (OFT)

Motor activity was measured in an open field test box (50 cm length 3 50 cm width 3 40 cm height). Mice were placed in the center of a plastic box in a room with dim light and were allowed to explore the arena for 15 min. All animal activity was recorded with an infrared camera placed above the box. Locomotion and time spent in the center during the last 10 min was measured (Ethovision XT software). The box was wiped clean with a paper towel soaked in 50% ethanol and dried thoroughly after each test session.

Elevated plus maze test (EPM)

The apparatus for the EPM consisted of two opposing open arms (44 cm length 3 12 cm width) and two closed arms (44 cm length 3 12 cm width), which were connected by a central zone (12 cm length 3 12 cm width). The whole apparatus was elevated 50 cm above the floor. The mouse was placed in the center zone facing toward one open arm and was allowed to freely explore the arena during a 6 min test session. Time spent in the open arm during the last 4 min was measured (Ethovision XT software). The box was wiped clean with a paper towel soaked in 50% ethanol and dried thoroughly after each test session.

Novelty-suppressed feeding test (NSF)

Food pellets were removed from the home cage for 24 h before testing (with ad libitum access to water). For testing, mice were placed in a corner of an unfamiliar white Plexiglas arena (50 cm length 3 50 cm width 3 40 cm height) with the floor covered in corn cob bedding under bright light conditions (~550 lux). A single food pellet placed on white filter paper (9 cm diameter) was prepositioned in the middle of the arena. The latency to eat was measured with a stopwatch and defined based on the first bite of the food pellet. The maximum time allowed was set at 10 min.

Chronic social defeat stress (CSDS)

Retired male breeder CD-1 mice were screened for aggressive behavior for 3 consecutive days and housed in the social defeat cage (26 cm width 3 45 cm depth 3 16 cm height) 24 h before the start of defeats on one side of a clear perforated Plexiglas divider (0.5 cm width 3 43 cm depth 3 16 cm height). C57BL/6 mice were subjected to physical interactions with an unfamiliar, aggressive CD-1 mouse for 10 min/day over 10 consecutive days. After interactions, C57BL/6 mice were removed and housed on the opposite side of the divider over the subsequent 24 h period. In the control group, C57BL/6 mice were housed two per cage on either side of a perforated divider and rotated daily in a similar manner without being exposed to the CD-1 mice. Experimental mice were singly housed after the last bout of physical interaction and the social interaction test was conducted 24 h later.

Social interaction test (SI)

Mice were first placed in an open arena (42 cm length 3 42 cm width 3 40 cm height) with an empty half-cylindrical metal cage (bottom diameter: 10 cm, height: 16 cm). Movements were recorded automatically for 2.5 min with a tracking system (Ethovision XT). Time spent in the area surrounding the cage (interaction zone, 8 cm region flanking cage) and in the area along the wall opposite to the cage (opposing zone, 9 cm region along wall opposing cage) was measured. Mice were then returned to the home cage for 30 s. Finally, a novel, aggressive CD1 mouse was placed in the cage and the same metrics were measured. The SI ratio was calculated by dividing the time spent in the interaction zone with CD1 mice divided by the time spent in the interaction zone without CD1 mice.

Chemogenetic manipulation

The designer drug CNO (2 mg/kg, i.p.; C0832, Sigma-Aldrich, St Louis, MO) was administrated 30 min before exposure to aversive stimuli (Figures 2E, 3A, and 5C) or social defeat stress (Figure S6A) or light therapy (7:30 AM, Figures 7A and S12A). For Figures 5D, S5A, S7A, CNO (2 mg/kg, i.p) was administrated between 10 AM – 10:30 AM.

QUANTIFICATION AND STATISTICAL ANALYSIS

Fiber photometry data analysis

Fiber photometry recording data were exported as MATLAB. Mat files from Spike2 software for further analysis. All raw data were smoothed with a moving average filter (20 ms span) and then segmented and aligned according to the onset of behavioral events within individual trials or bouts. The fluorescence change (DF/F) values were calculated as $(F-F_0)/F_0$, where F_0 is the baseline fluorescence signal averaged over a 1.5 s-long control time window (typically set 0.5 s) prior to a trigger event. DF/F values are presented as heatmaps or as average plots with a shaded area indicating the SEM. A multivariate permutation test was used to analyze the statistical significance of the event-related fluorescence change (ERF). Then, 1,000 permutations for an a-level of 0.05 were used to compare the values of DF/F at each time point with the ERF baseline values.

Quantification of neurons infected with different viruses

To quantify the percentage of RV-DsRed-labeled RGCs co-labeled with SMI-32 (Figure 4E), 4 C57BL/6 mice received vLGN/IGL injection of helper virus and LHb injection of SAD-DG-DsRed (EnvA) were used. In each mouse, the numbers of RV-DsRed-labeled RGCs and RV-DsRed/SMI-32 double-labeled RGCs were counted in the contralateral retina. The percentage of RV-DsRed/SMI-32 double-labeled RGCs was calculated as the percentage of the total number of RV-DsRed/SMI-32 double-labeled RGCs counted in 4 mice within the total number of RV-DsRed-labeled RGCs counted in 4 mice.

To quantify the percentage of RV-DsRed-labeled RGCs co-labeled with eYFP (Figure 4F), 3 Opn4-Cre mice received vLGN/IGL injection of helper virus, LHb injection of SAD-DG-DsRed (EnvA), and intraocular injection of AAV2/9-Ef1a-DIO-eYFP were used. In each mouse, the numbers of RV-DsRed-labeled RGCs and RV-DsRed/eYFP double-labeled RGCs were counted in the contralateral retina. The percentage of RV-DsRed/eYFP double-labeled RGCs was calculated as the percentage of the total number of RV-DsRed/eYFP double-labeled RGCs counted in 3 mice within the total number of RV-DsRed-labeled RGCs counted in 3 mice.

To quantify the percentage of LHb-projecting vLGN/IGL neurons co-labeled with retrobeads and mCherry (Figure S1A), 3 vGAT-Cre mice received vLGN/IGL injection of AAV2/9-hSyn-DIO-mCherry and LHb injection of green retrobeads were used. In each mouse, the numbers of retrobeads-labeled neurons and retrobeads/mCherry double-labeled neurons were counted in 4 consecutive brain sections (40 ㎜/section) across the vLGN/IGL. The percentage of retrobeads/mCherry double-labeled neurons was calculated as the percentage of the total number of retrobeads/mCherry double-labeled neurons counted in 3 mice within the total number of retrobeads-labeled neurons counted in 3 mice.

To quantify the percentage of LHb postsynaptic neurons co-labeled with eYFP and CaMKIIa (Figure S1B), 4 C57BL/6 mice received vLGN/IGL injection of AAV2/1-hSyn-Cre and LHb injection of AAV2/9-Ef1a-DIO-eYFP were used. In each mouse, the numbers of eYFP-labeled neurons and eYFP/CaMKIIa double-labeled neurons were counted in 4 consecutive brain sections (40 ㎜/section) across the LHb. The percentage of eYFP/CaMKIIa double-labeled neurons was calculated as the percentage of the total number of eYFP/CaMKIIa double-labeled neurons counted in 4 mice within the total number of eYFP-labeled neurons counted in 4 mice.

To quantify the percentage of LHb postsynaptic neurons co-labeled with eYFP and red retrobeads (Figures S2H and S2L), 6 C57BL/6 mice received vLGN/IGL injection of AAV2/1-hSyn-Cre, LHb injection of AAV2/9-Ef1a-DIO-eYFP, and DRN (n = 3 mice) or VTA (n = 3 mice) injection of red retrobeads were used. In each mouse, the numbers of eYFP-labeled neurons and eYFP/retrobeads double-labeled neurons were counted in 4 consecutive brain sections (40 ㎜/section) across the LHb. The percentage of eYFP/retrobeads double-labeled neurons was calculated as the percentage of the total number of eYFP/retrobeads double-labeled neurons counted in 3 mice within the total number of eYFP-labeled neurons counted in 3 mice.

To quantify the numbers of starter cells in the vLGN/IGL and RV-DsRed-labeled presynaptic RGCs in the retina (Figure S8B), 6 C57BL/6 mice received vLGN/IGL injection of helper virus and LHb injection of SAD-DG-DsRed (EnvA) were used. In each mouse, the numbers of helper virus/RV-DsRed double-labeled starter cells from 4 consecutive brain sections (40 ㎜/section) across the vLGN/IGL, and RV-DsRed-labeled RGCs from the contralateral retina were counted. The average number of starter cells in the vLGN/IGL and RV-DsRed-labeled presynaptic RGCs in the retina was calculated as the total number of starter cells and presynaptic RGCs counted in 6 animals divided by the number of animals.

Quantification of c-Fos immunostaining

To quantify the influence of chemogenetic activation of LHb-projecting vLGN/IGL neurons on c-Fos expression (Figure 2B), 12 C57BL/6 mice that received LHb injection of rAAV2/2-hSyn-Retro-Cre and vLGN/IGL injection of AAV2/9-hSyn-DIO-hM3D(Gq)-mCherry were divided into 2 groups: 1) Saline, 6 mice received i.p. injection of saline, followed by a 30 min interval and then received light deprivation (2 h); 2) CNO, 6 mice received i.p. injection of CNO, followed by a 30 min interval and then received light deprivation (2 h). All animals were anaesthetized and perfused. Brain slices across the vLGN/IGL were subjected to immunostaining for c-Fos.

In each mouse, the numbers of hM3D-labeled neurons and c-Fos/hM3D double-labeled neurons were counted from 4 consecutive brain sections (40 μm/section) across the vLGN/IGL. The percentage of c-Fos/hM3D double-labeled neurons in each group was calculated as the percentage of the total number of c-Fos/hM3D double-labeled neurons counted in 6 mice within the total number of hM3D-labeled neurons counted in 6 mice.

To quantify the influence of chemogenetic activation of vLGN/IGL-projecting RGCs on c-Fos expression (Figure 5B), 10 C57BL/6 mice that received vLGN/IGL injection of rAAV2/2-hSyn-Retro-Cre and intraocular injection of AAV2/9-hSyn-DIO-hM3D(Gq)-mCherry were divided into 2 groups: 1) Saline, 5 mice received i.p. injection of saline, followed by a 30 min interval and then received light deprivation (2 h); 2) CNO, 5 mice received i.p. injection of CNO, followed by a 30 min interval and then received light deprivation (2 h). All animals were anaesthetized and perfused. Retinas were subjected to immunostaining for c-Fos. In each mouse, the numbers of hM3D-labeled RGCs and c-Fos/hM3D double-labeled RGCs were counted. The percentage of c-Fos/hM3D double-labeled RGCs in each group was calculated as the percentage of the total number of c-Fos/hM3D double-labeled RGCs counted in 5 mice within the total number of hM3D-labeled RGCs counted in 5 mice.

To quantify the influence of chemogenetic inhibition of LHb postsynaptic neurons on c-Fos expression (Figure S4C), 12 C57BL/6 mice that received vLGN/IGL injection of AAV2/1-hSyn-Cre and LHb injection of AAV2/9-hSyn-DIO-hM4D(Gi)-mCherry were divided into 2 groups: 1) Saline-AS, 6 mice received i.p. injection of saline, followed by a 30 min interval and then exposure to foot shock (1 mA, 500 ms); 2) CNO-AS, 6 mice received i.p. injection of CNO, followed by a 30 min interval and then exposure to foot shock (1 mA, 500 ms). After a 2 h interval, all animals were anaesthetized and perfused. Brain slices across the LHb were subjected to immunostaining for c-Fos. In each mouse, the numbers of hM4D-labeled neurons and c-Fos/hM4D double-labeled neurons were counted from 4 consecutive brain sections (40 μm/section) across the LHb. The percentage of c-Fos/hM4D double-labeled neurons in each group was calculated as the percentage of the total number of c-Fos/hM4D double-labeled neurons counted in 6 mice within the total number of hM4D-labeled neurons counted in 6 mice.

To quantify the influence of acute light exposure on c-Fos expression in the vLGN/IGL, LHb, periaqueductal gray (PAG) and amygdala (Figures S10C and S10D), 16 C57BL/6 mice were divided into 4 groups: 1) RL, 4 mice exposed to room light (7 AM – 11 AM, 120 lux); 2) RL+LT, 4 mice that first exposed to room light (7 AM – 9 AM) and then exposed to light therapy (9 AM – 11 AM, 3000 lux); 3) Dark, 4 mice received light deprivation (7 AM – 11 AM); 4) Dark+LT, 4 mice that first received light deprivation (7 AM – 9 AM) and then exposed to light therapy (9 AM – 11 AM, 3000 lux). All animals were anaesthetized and perfused. Brain slices across the vLGN/IGL, LHb, PAG and amygdala were subjected to immunostaining for c-Fos. In each mouse, the numbers of c-Fos+ cells were counted from 4 consecutive brain sections (40 μm/section) across the vLGN/IGL, LHb, PAG and amygdala, respectively. The average number of c-Fos+ cells in the vLGN/IGL, LHb, PAG and amygdala (basolateral amygdala and central amygdala) was calculated as the total number of c-Fos+ cells counted in 4 animals divided by the number of animals.

To quantify the influence of chemogenetic inhibiton of LHb-projecting vLGN/IGL neurons on c-Fos expression (Figure S11A), 18 C57BL/6 mice that received LHb injection of rAAV2/2-hSyn-Retro-Cre and vLGN/IGL injection of AAV2/9-hSyn-DIO-hM4D(Gi)-mCherry were divided into 3 groups: 1) D-Saline, 6 mice received i.p. injection of saline and light deprivation (2 h); 2) LT-Saline, 6 mice received i.p. injection of saline and light therapy (3000 lux, 2 h); 3) LT-CNO, 6 mice received i.p. injection of CNO and light therapy (3000 lux, 2 h). All animals were anaesthetized and perfused. Brain slices across the vLGN/IGL were subjected to immunostaining for c-Fos. In each mouse, the numbers of hM4D-labeled neurons and c-Fos/hM4D double-labeled neurons were counted from 4 consecutive brain sections (40 μm/section) across the vLGN/IGL. The percentage of c-Fos/hM4D double-labeled neurons in each group was calculated as the percentage of the total number of c-Fos/hM4D double-labeled neurons counted in 6 mice within the total number of hM4D-labeled neurons counted in 6 mice.

To quantify the influence of chemogenetic activation of LHb postsynaptic neurons on c-Fos expression (Figure S11B), 18 C57BL/6 mice that received vLGN/IGL injection of AAV2/1-hSyn-Cre and LHb injection of AAV2/9-hSyn-DIO-hM3D(Gq)-mCherry were divided into 3 groups: 1) D-Saline, 6 mice received i.p. injection of saline and light deprivation (2 h); 2) D-CNO, 6 mice received i.p. injection of CNO and light deprivation (2 h); 3) LT-CNO, 6 mice received i.p. injection of CNO and light therapy (3000 lux, 2 h). All animals were anaesthetized and perfused. Brain slices across the LHb were subjected to immunostaining for c-Fos. In each mouse, the number of hM3D-labeled neurons and c-Fos/hM3D double-labeled neurons were counted from 4 consecutive brain sections (40 μm/section) across the LHb. The percentage of c-Fos/hM3D double-labeled neurons in each group was calculated as the percentage of the total number of c-Fos/hM3D double-labeled neurons counted in 6 mice within the total number of hM3D-labeled neurons counted in 6 mice.

To quantify the influence of chemogenetic inhibition of vLGN/IGL-projecting RGCs on c-Fos expression (Figure S11C), 18 C57BL/6 mice that received vLGN/IGL injection of rAAV2/2-hSyn-Retro-Cre and intraocular injection of AAV2/9-hSyn-DIO-hM4D(Gi)-mCherry were divided into 3 groups: 1) D-Saline, 6 mice received i.p. injection of saline and light deprivation (2 h); 2) LT-Saline, 6 mice received i.p. injection of saline and light therapy (3000 lux, 2 h); 3) LT-CNO, 6 mice received i.p. injection of CNO and light therapy (3000 lux, 2 h). All animals were anaesthetized and perfused. Retinas were subjected to immunostaining for c-Fos. In each mouse, the numbers of hM4D-labeled RGCs and c-Fos/hM4D double-labeled RGCs were counted. The percentage of c-Fos/hM4D double-labeled RGCs in each group was calculated as the percentage of the total number of c-Fos/hM4D double-labeled RGCs counted in 6 mice within the total number of hM4D-labeled RGCs counted in 6 mice.

Please cite this article in press as: Huang et al., A Visual Circuit Related to Habenula Underlies the Antidepressive Effects of Light Therapy, Neuron (2019), https://doi.org/10.1016/j.neuron.2019.01.037

Statistics

All statistics were calculated using GraphPad Prism 7 software. Data analysis was performed by experimenters blind to experimental conditions. Statistical details including the definitions and exact value of n (e.g., number of animals, number of neurons, etc), p values, and the types of the statistical tests can be found in the Figures and Figure legends. One-way ANOVA was used to evaluate frequency changes, number of c-Fos+ cells, and peak DF/F. One-way ANOVA and then Sidak's multiple comparisons test were used to quantify depressive- and anxiety-like behaviors, number of action potentials related to current injection, and spontaneous firing frequency of LHb neurons. Chi-square test was used to quantify the percentage of burst-firing cells. For all figures, dot plots include a horizontal line representing the mean. Statistical significance was set at $p < 0.05$.